Integrating the Pressure-Sensitive Nonassociative Plasticity by Exponential-Based Methods

Mohammad Rezaiee-Pajand
Professor of Civil Engineering,
Ferdowsi University of Mashhad,
Mashhad, 91775-1111 Iran

Mehrdad Sharifian
Ph.D. Student of Structural Engineering

Mehrzad Sharifian
Ph.D. Structural Engineering

Ferdowsi University of Mashhad,
Mashhad, 91775-1111 Iran

A nonassociative plasticity model of Drucker–Prager yield surface coupled with a generalized nonlinear kinematic hardening is considered. Conforming to the plasticity model, two exponential-based methods, called fully explicit and semi-implicit, are recommended for integrating its constitutive equations. These techniques are proposed for the first time to solve nonlinear hardening materials. The integrations are thoroughly investigated by utilizing stress and strain-updating tests along with a boundary value problem in diverse grounds of accuracy, convergence rate, and efficiency. The results indicate that the fully explicit scheme is more accurate and efficient than the Euler's, but the same convergence rate as the classical integrations is also perceived. Having a quadratic convergence, the semi-implicit is noticeably the most accurate and efficient procedure to use for this plasticity model among the algorithms in question. Since the plasticity model is in a great consistency with discontinuously reinforced aluminum (DRA) composites, the suggested formulations can be utilized pragmatically. The tangent moduli of the proposed and Euler's strategies are derived and examined, as well, due to their vital role in achieving the asymptotic quadratic convergence rate of the Newton–Raphson solution in nonlinear finite-element analyses. [DOI: 10.1115/1.4024173]

Keywords: plasticity, exponential-based integration, Drucker–Prager's criterion, tangent modulus

1 Introduction

The prevailing account of metallic materials was that they are pressure independent and as a result the associative plasticity models were taken into account in their nonlinear analyses. This is one of the basic tenets of the classical metal plasticity based on the Bridgman's works [1,2]. In subsequent investigations, different experiments demonstrated that there are also a considerable number of metallic materials being pressure sensitive and declining the conventional account.

For instance, Spitzig et al. [3,4] performed the basic researches in this ground where they examined the stress–strain behavior of high-strength steels like AISI 4310, AISI 4330, and HY-80 to show the pressure sensitivity of their yield and flow stresses. Spitzig and Richmond [5] proved that iron-based materials and aluminum are also sensitive to hydrostatic pressure with a linear relationship between flow stress and hydrostatic pressure and incompressible plastic deformation. This fact was also confirmed by Wilson [6]. Examining 2024-T351 aluminum and using nonlinear finite-element analysis, he demonstrated that the Drucker–Prager yield criterion [7] essentially matched the experimental results while the results of von-Mises were overestimated. Subsequently, Singh et al. [8] concluded that the pressure dependence flow stress model by Spitzig and Richmond [5] appeared the most promising since it gave a relatively better agreement with most of the experimental observations. Improving the elastoplastic theory for grey cast iron, Altenbach et al. [9] experimentally showed that the elastoplastic behavior of the material cannot be described using classical approaches and there is also sensitivity to the influence of the hydrostatic pressure on the plastic behavior. They also deduced that there should be a nonassociative flow rule with employing a plastic potential to have a good agreement with experiments. The same results were also concluded by Chait [10] for Titanium alloys, and by Gil et al. [11], Iyer and Lissenden [12], and Lewandowski et al. [13] for nickel base alloys such as Inconel 718.

The aforementioned characteristics for these metallic materials lead to a certain plasticity model where the flow rule is nonassociative, and the plastic deformation is incompressible. Conforming to this account, Lei and Lissenden [14] presented a plasticity model for DRA composites, which particularly suits their experimental results and also the work of others. These composites are widely used metallic materials showing the same characteristics as the aforementioned metals. Some of their great features are specific stiffness, tailorable thermal expansion coefficient, ductility, and wear resistance. The plasticity model consists of a Drucker–Prager yield criterion, a nonassociative flow rule with incompressible plastic deformation, and a generalized nonlinear kinematic hardening. As a significant part of this plasticity whose integrations will be discussed, here, a brief account of the developments of the kinematic hardening rules is presented.

Prager proposed the simplest kinematic hardening asserting that the direction of the plastic strain increment is the same as the back stress evolution [15,16]. His linear kinematic hardening could appropriately predict the Bauschinger effect in cyclic loading. However, the nonlinear kinematic hardenings are required to forebode ratcheting whenever a structure undergoes a cyclic load. Generally, the hardening rules can be categorized into two general types of coupled and uncoupled models corresponding to the defined kinematic hardening mechanism which is coupled or uncoupled with the plastic modulus [17]. For the coupled, several models can be addressed by Armstrong and Frederick [18], Chaboche [19,20], Ohno and Wang [21], Abdel-Karim and Ohno [22], Kang [23], Chaboche [24], Abdel-Karim [25], and Rezaiee-Pajand and Siniae [26]. The kinematic hardening rules proposed by Mroz [27], Dafalias and Popov [28], and Tseng and Lee [29] are placed in the category of the uncoupled models.

The material's constitutive equations characterize the stress as a function of the deformation history. Integrating these equations, stresses are updated and an important part of the nonlinear finite-

Contributed by the Materials Division of ASME for publication in the Journal of Engineering Materials and Technology. Manuscript received June 4, 2012; final manuscript received January 18, 2013; published online May 13, 2013. Assoc. Editor: Marwan K. Khraisheh.

Copyright © 2013 by ASME

Downloaded From: http://materialstechnology.asmedigitalcollection.asme.org/ on 05/25/2013 Terms of Use: http://asme.org/terms

element analysis is fulfilled. Although the analytical exact integrating methods [30–37] have been developed for a few plasticity models and are rarely used for their restrictions, still the general approach is utilizing the numerical integrations due to their universality, flexibility and tolerance toward all kinds of materials and plasticity models. The problem is, though, these approximate procedures usually involve many iterations and calculations, and their accuracy and performance are in a direct relationship with the final outcomes of the nonlinear analyses. Therefore, it is of great importance to use the numerical integrating algorithms with as much accuracy and efficiency as possible.

In overall, the integrating schemes are divided into two general groups of implicit and explicit algorithms. The return mapping integration schemes proposed by Wilkins [38], Rice and Tracey [39], and Ortiz and Popov [40] are samples of the implicit cluster of integrating tactics. In the recent decade, the implicit backward Euler integrating scheme, which is one of the well-known return mapping techniques, was extended for different types of plastic constitutive models by Kobayashi and Ohno [41], Kobayashi et al. [42], Kang [43], Kan et al. [44], and Coombs et al. [45].

The forward Euler (FE) formulation is a famous classical technique among the explicit integrations. Another group of explicit formulations, introduced in the recent decade, are exponential-based integrations. These methodologies are developed in an augmented stress space through an additional component of time in the Minkowski space-time. Investigating the characteristics of the Minkowski space-time, Hong and Liu [46–48] argued that the constitutive equations of the von-Mises plasticity with linear kinematic hardening could be represented by a system of linear differential equations. Liu [49–51] developed the method for the von-Mises mixed-hardening and Drucker–Prager plasticity. Another integration process based on the exponential map techniques was developed by Auricchio and Beirão da Veiga [52] to solve the constitutive equations of the von-Mises plasticity model with a linear mixed-hardening mechanism. Artioli et al. [53] improved their integrating algorithm into two consistent exponential-based tactics consistent with the yield condition. Enhancing the algorithm from a first-order scheme to second-order integrations, Artioli et al. [54,55] and Rezaiee-Pajand and Nasirai [56] presented exponential-based integrations of second-order accuracy for von-Mises plasticity model with linear isotropic and kinematic hardening. Rezaiee-Pajand and Nasirai [57] followed the effort by presenting a numerical scheme based on exponential maps for integrating the constitutive equations of the Drucker–Prager plasticity model with no hardening. Considering the von-Mises plasticity model with a class of multicomponent nonlinear kinematic hardening, Rezaiee-Pajand et al. [58,59] developed the exponential-based formulations and extended them to nonlinear mixed-hardening models. Recently, two new exponential-based approximate formulations for associative Drucker–Prager plasticity model were developed by Rezaiee-Pajand et al. [36] assuming linear hardening. They also derived an accurate solution for the constitutive equations.

As a practical objective, in this study, the plasticity model proposed by Lei and Lissenden [14] is considered. This model consists of a nonassociative Drucker–Prager yield criterion with Chaboche's nonlinear kinematic hardening and incompressible plastic deformation. This plasticity model is in a great correlation with the DRA composites which inspired the authors to develop two consistent exponential-based methods for integrating their constitutive equations. These two schemes were first devised in Refs. [51,57] for the Drucker–Prager plasticity with no hardening. In this investigation, they are advanced for the nonassociative Drucker–Prager plasticity with nonlinear kinematic hardening, which are totally new and had never been carried out before. Considering a broad range of numerical tests, including stress and strain-updating assessments alongside a boundary value problem, the results of the suggested algorithms are compared to those of the classical integrations, Backward and Forward Euler's tactics. To investigate the computational efficiency or performance of the formulations, accuracy and computational times of the proposed algorithms and Euler's integrations are computed and compared. Having developed the consistent tangent moduli of the developed schemes and the Euler's, their accuracy and asymptotic quadratic convergence rate, when used with a Newton–Raphson solution, are examined.

Simplifying the presentation of the formulations, all second-order tensors are represented by nine-component column vectors via arranging the tensor components in a vector format. Symmetry of the second-order tensors contributes to six independent components in each vector, which is a great aid. It is also worth mentioning that the definition of the trace operator and the Euclidean norm need to be modified.

2 Basic Models

To develop the required basic equations, it is considered a non-associative Drucker–Prager plasticity model with nonlinear kinematic hardening and the plastic deformation which is incompressible. The strains are assumed in the realm of small strains. The Drucker–Prager yield surface can consider the hydrostatic pressure effect on failure through the second term of its relationship, which is an asset to the von-Mises, as follows:

$$F = \frac{1}{2}\mathbf{s}'^{\mathrm{T}}\mathbf{s}' - (\tau_{\mathrm{y}} - \beta p')^2 = 0, \quad \tau_{\mathrm{y}} - \beta p' > 0 \tag{1}$$

In this relationship, $\mathbf{s}'$ and p' are deviatoric and hydrostatic parts of the shifted stress, respectively. The parameter τ_y is dubbed yield stress in pure shear, and β is a material constant. The shifted stress is defined as a result of deducting the back stress vector, $\mathbf{a}$, from the total stress vector, $\boldsymbol{\sigma}$. The shifted stress, $\boldsymbol{\sigma}'$, and the total strain, $\boldsymbol{\varepsilon}$, vectors are decomposed into their deviatoric and volumetric parts. The volumetric shifted stress, also called the hydrostatic shifted stress, is subjected to volumetric part of the strain with proportion factor of the material bulk modulus, K. The followings are the related relationships existing between these parameters:

$$\boldsymbol{\sigma}' = \boldsymbol{\sigma} - \mathbf{a} \tag{2}$$

$$\boldsymbol{\sigma}' = \mathbf{s}' + p'\mathbf{i} \quad \text{with} \quad p' = \frac{\mathrm{tr}(\boldsymbol{\sigma}')}{3} \tag{3}$$

$$\boldsymbol{\varepsilon} = \mathbf{e} + \frac{\varepsilon_{\mathrm{v}}}{3}\mathbf{i} \quad \text{with} \quad \varepsilon_{\mathrm{v}} = \mathrm{tr}(\boldsymbol{\varepsilon}) \tag{4}$$

$$p = K\varepsilon_{\mathrm{v}} \tag{5}$$

where $\mathbf{e}$ and ε_{v} are the deviatoric and volumetric parts of the total strain, $\boldsymbol{\varepsilon}$. To build up the framework, it is needed for these parameters to be divided into their elastic and plastic parts, as follows:

$$\boldsymbol{\varepsilon} = \boldsymbol{\varepsilon}^{\mathrm{e}} + \boldsymbol{\varepsilon}^{\mathrm{p}} \tag{6}$$

$$\mathbf{e} = \mathbf{e}^{\mathrm{e}} + \mathbf{e}^{\mathrm{p}} \tag{7}$$

$$\varepsilon_{\mathrm{v}} = \varepsilon_{\mathrm{v}}^{\mathrm{e}} + \varepsilon_{\mathrm{v}}^{\mathrm{p}} \tag{8}$$

The rate of the plastic strain is defined by the following equation:

$$\dot{\boldsymbol{\varepsilon}}^{\mathrm{p}} = \dot{\gamma}\frac{\partial Q}{\partial \boldsymbol{\sigma}'} \tag{9}$$

where $\dot{\gamma}$ and Q are known as the plastic multiplier and plastic potential, respectively. Note that in this equation and all other comings, the superposed dot introduces that the denoted parameter is contingent on the pseudotime. Pseudotime is defined as a response to the need for visualizing the stress and strain histories. From now on, for short, pseudotime is called time. In this study, the flow rule is nonassociative. As a result, the function of the yield surface, F, cannot be employed as the plastic potential.

Downloaded From: http://materialstechnology.asmedigitalcollection.asme.org/ on 05/25/2013 Terms of Use: http://asme.org/terms

Hiring the von-Mises yield function, the potential is defined by the next relation

$$Q = \frac{1}{2}\mathbf{s}'^{\mathrm{T}}\mathbf{s}' \tag{10}$$

Using Eqs. (9) and (10), the plastic strain rate is achieved as

$$\dot{\boldsymbol{\varepsilon}}^{\mathrm{p}} = \dot{\gamma}\mathbf{s}' \tag{11}$$

Due to incompressible plastic deformation, the volumetric part of the plastic strain vanishes, which leads to the next result

$$\dot{\varepsilon}_{\mathrm{v}}^{\mathrm{p}} = 0 \rightarrow \dot{\boldsymbol{\varepsilon}}^{\mathrm{p}} = \dot{\mathbf{e}}^{\mathrm{p}} \tag{12}$$

Merging Eqs. (11) and (12), the subsequent connection will form

$$\dot{\mathbf{e}}^{\mathrm{p}} = \dot{\gamma}\mathbf{s}' \tag{13}$$

To regulate the evolution of the back stress, the succeeding Chaboche's nonlinear kinematic hardening is adopted

$$\dot{\mathbf{a}} = \sum_{i=1}^{m} \dot{\mathbf{a}}_i \tag{14}$$

$$\dot{\mathbf{a}}_i = H_{\mathrm{kin},i}\dot{\boldsymbol{\varepsilon}}^{\mathrm{p}} - H_{\mathrm{nl},i}\dot{\gamma}\mathbf{a}_i \tag{15}$$

where m specifies the number of components of the back stress, $H_{\mathrm{kin},i}$ is a material constant called kinematic hardening modulus signifying strain hardening, and $H_{\mathrm{nl},i}$ shows the nonlinearity of the considered kinematic hardening. The latter factor is also a constant parameter pertaining to the type of the material.

Since the framework is formulated in deviatoric space, the deviatoric back stress is required to be obtained by the following formulae:

$$\boldsymbol{\alpha} = \mathbf{a} - \frac{\mathrm{tr}(\mathbf{a})}{3}\mathbf{i} \tag{16}$$

$$\dot{\boldsymbol{\alpha}} = \sum_{i=1}^{m} \dot{\boldsymbol{\alpha}}_i \tag{17}$$

$$\dot{\boldsymbol{\alpha}}_i = H_{\mathrm{kin},i}\dot{\mathbf{e}}^{\mathrm{p}} - H_{\mathrm{nl},i}\dot{\gamma}\boldsymbol{\alpha}_i \tag{18}$$

Using generalized Hooke's law, the rate of the shifted stress is derived as a function of strain

$$\dot{\boldsymbol{\sigma}}' = 2G\dot{\boldsymbol{\varepsilon}}^{\mathrm{e}} + \left(K - \frac{2}{3}G\right)\dot{\varepsilon}_{\mathrm{v}}^{\mathrm{e}}\mathbf{i} - \sum_{i=1}^{m}\left(H_{\mathrm{kin},i}\dot{\boldsymbol{\varepsilon}}^{\mathrm{p}} - H_{\mathrm{nl},i}\dot{\gamma}\mathbf{a}_i\right) \tag{19}$$

Substituting $\mathbf{a}_i$ from Eq. (16) in Eq. (19) and comparing with Eqs. (3) and (4) result in the following relationships for the rate of the deviatoric, $\dot{\mathbf{s}}'$, and volumetric, $\dot{p}'$, parts of the shifted stress, $\boldsymbol{\sigma}'$:

$$\dot{\mathbf{s}}' = 2\mathrm{G}\dot{\mathbf{e}}^{\mathrm{e}} - \sum_{i=1}^{m}\left(H_{\mathrm{kin},i}\dot{\mathbf{e}}^{\mathrm{p}} - H_{\mathrm{nl},i}\dot{\gamma}\boldsymbol{\alpha}_i\right) \tag{20}$$

$$\dot{p}' = K\dot{\varepsilon}_{\mathrm{v}}^{\mathrm{e}} + \sum_{i=1}^{m} H_{\mathrm{nl},i}\dot{\gamma}\frac{\mathrm{tr}(\mathbf{a}_i)}{3} \tag{21}$$

Employing Eqs. (7) and (13) with a little manipulation, Eq. (20) can be rewritten in the following form:

$$\dot{\mathbf{s}}' = 2G\dot{\mathbf{e}} - 2G\dot{\gamma}\mathbf{s}' - \dot{\gamma}\mathbf{s}'\sum_{i=1}^{m} H_{\mathrm{kin},i} + \dot{\gamma}\sum_{i=1}^{m} H_{\mathrm{nl},i}\boldsymbol{\alpha}_i \tag{22}$$

The coming relationships are the loading/unloading conditions in Kuhn–Tucker complementary form. These conditions are used to determine if the material is in the plastic or elastic phase. If $\dot{\gamma} = 0$ and $F \le 0$, the material is in the elastic phase, and once the condition $\dot{\gamma} > 0$ and $F = 0$ is met, the material is in the plastic phase

$$\dot{\gamma} \ge 0, \quad F \le 0, \quad \dot{\gamma}F = 0 \tag{23}$$

Employing the consistency condition

$$\dot{\gamma}\dot{F} = 0 \quad \text{if} \quad F = 0, \tag{24}$$

alongside Eqs. (1) and (22), the plastic multiplier is acquired, as follows:

$$\dot{\gamma} = \frac{2G\dot{\mathbf{e}}^{\mathrm{T}}\mathbf{s}' + 2\beta K(\tau_y - \beta p')\dot{\varepsilon}_{\mathrm{v}}}{\left(4G + 2\sum_{i=1}^{m} H_{\mathrm{kin},i}\right)(\tau_y - \beta p')^2 - \mathbf{s}'^{\mathrm{T}}\sum_{i=1}^{m} H_{\mathrm{nl},i}\boldsymbol{\alpha}_i} \tag{25}$$

The last equality can be oversimplified having defined the constant parameter $\bar{G}$ and also used the yield-surface radius, R, as

$$2\bar{G} = 2G + \sum_{i=1}^{m} H_{\mathrm{kin},i} \tag{26}$$

and

$$R = \sqrt{2}(\tau_{\mathrm{y}} - \beta p') \tag{27}$$

into

$$\dot{\gamma} = \frac{2G\dot{\mathbf{e}}^{\mathrm{T}}\mathbf{s}' + \sqrt{2}\beta KR\dot{\varepsilon}_{\mathrm{v}}}{2\bar{G}R^2 - \mathbf{s}'^{\mathrm{T}}\sum_{i=1}^{m} H_{\mathrm{nl},i}\boldsymbol{\alpha}_i} \tag{28}$$

3 Exponential Map Integration

In this study, it is desired to develop two consistent exponential mapping methods for integrating nonassociative Drucker–Prager's constitutive equations with nonlinear kinematic hardening and incompressible plastic deformation. To develop the proposed algorithm based on the exponential concept, the original constitutive differential equations must be converted into quasi-linear ones. Mapping the original differential problem into an augmented stress space and defining an integrating factor, the task is performed and the following dynamical system will be the result:

$$\dot{\mathbf{X}} = \mathbb{A}\mathbf{X} \tag{29}$$

where $\mathbf{X}$ is the augmented stress vector and $\mathbb{A}$ is dubbed the control matrix. This is an equivalent but rather different form of the initial differential problem, which has been improved to be conveniently solvable.

Equation (22) is simplified and reformed to the next relationship having multiplied the both sides by integrating factor X^0 and hired the parameter $\bar{G}$. It is also assumed for the integrating factor to satisfy the subsequent multiple equalities as though the first two parts could be derived from the third part

$$X^0\dot{\mathbf{s}}' + 2\bar{G}\dot{\gamma}X^0\mathbf{s}' = 2GX^0\dot{\mathbf{e}} + \dot{\gamma}X^0\sum_{i=1}^{m} H_{\mathrm{nl},i}\boldsymbol{\alpha}_{n,i} = \frac{\mathrm{d}}{\mathrm{d}t}(X^0\mathbf{s}') \tag{30}$$

Considering the first and last parts of the former relation, also the middle and last ones, one can draw out the next two equations

$$\dot{X}^0\mathbf{s}' + X^0\dot{\mathbf{s}}' = X^0\dot{\mathbf{s}}' + 2\bar{G}\dot{\gamma}X^0\mathbf{s}' \tag{31}$$

$$\frac{\mathrm{d}}{\mathrm{d}t}(X^0\mathbf{s}') = 2GX^0\dot{\mathbf{e}} + \dot{\gamma}X^0\sum_{i=1}^{m} H_{\mathrm{nl},i}\boldsymbol{\alpha}_{n,i} \tag{32}$$

Downloaded From: http://materialstechnology.asmedigitalcollection.asme.org/ on 05/25/2013 Terms of Use: http://asme.org/terms

Removing the similar segments from the both sides of the Eq. (31) gives rise to the coming relationship, from which the integrating factor is obtained

$$X^0 = \exp(2\bar{G}\gamma) \tag{33}$$

It is helpful to mention that the initial condition of $X^0(\gamma = 0) = 1$ has been taken into account to derive this relationship. The reason is that, the material is undisturbed at the beginning of the loading process. Considering the Drucker–Prager's yield function and Eq. (27), the following equalities are formed:

$$R^2 = \mathbf{s}'^{\mathrm{T}}\mathbf{s}' \quad \& \quad \dot{R}R = \dot{\mathbf{s}}'^{\mathrm{T}}\mathbf{s}' \tag{34}$$

Having utilized the previous relationships and multiplied the middle and last parts of Equality (30) by $\mathbf{s}'^{\mathrm{T}}$, the subsequent differential equation is derived

$$\frac{\mathrm{d}}{\mathrm{d}t}(X^0 R) = \frac{2G}{R}X^0\mathbf{s}'^{\mathrm{T}}\dot{\mathbf{e}} + \frac{\dot{\gamma}X^0}{R}\mathbf{s}'^{\mathrm{T}}\sum_{i=1}^{m} H_{\mathrm{nl},i}\boldsymbol{\alpha}_{n,i} \tag{35}$$

At this stage, there is a set of differential equations in the augmented stress space, Eqs. (32) and (35). Getting into these relationships, it can be perceived that a fixed term of parameters is recurred in both. Choosing a variable as a representative of this term helps the equations be much more comprehensible. The mentioned term is given below

$$\dot{\boldsymbol{\mu}} = \dot{\mathbf{e}} + \frac{\dot{\gamma}}{2G}\sum_{i=1}^{m} H_{\mathrm{nl},i}\boldsymbol{\alpha}_{n,i} \tag{36}$$

Hence, the differential equations are transformed to the following condensed ones:

$$\frac{\mathrm{d}}{\mathrm{d}t}(X^0\mathbf{s}') = 2GX^0\dot{\boldsymbol{\mu}} \tag{37}$$

$$\frac{\mathrm{d}}{\mathrm{d}t}(X^0 R) = \frac{2G}{R}X^0\dot{\boldsymbol{\mu}}^{\mathrm{T}}\mathbf{s}' \tag{38}$$

These differential equations can be suited into the below generalized shape

$$\dot{\mathbf{X}} = \mathbb{A}\mathbf{X} \Leftrightarrow \frac{\mathrm{d}}{\mathrm{d}t}\begin{Bmatrix} \mathbf{X}^{\mathrm{S}} \\ X^{\mathrm{R}} \end{Bmatrix} = \begin{bmatrix} \mathbb{O}_{9\times 9} & \dfrac{2G}{R}\dot{\boldsymbol{\mu}} \\ \dfrac{2G}{R}\dot{\boldsymbol{\mu}}^{\mathrm{T}} & 0 \end{bmatrix}_{10\times 10} \begin{Bmatrix} \mathbf{X}^{\mathrm{S}} \\ X^{\mathrm{R}} \end{Bmatrix} \tag{39}$$

where $\mathbf{X}^{\mathrm{S}}$ and X^{R} are the components of the augmented stress vector defined as follows:

$$\mathbf{X}^{\mathrm{S}} = X^0\mathbf{s}' \quad \& \quad X^{\mathrm{R}} = X^0 R \tag{40}$$

Pursuing below conditions, one can manage to distinguish between the elastic and plastic phases. Material has entered the plastic stage once the both are simultaneously fulfilled; otherwise, it is still in the elastic phase.

(1) $\|\mathbf{s}'\|^2 = R^2$, i.e., $\|\mathbf{X}^{\mathrm{S}}\|^2 = (X^{\mathrm{R}})^2$.
(2) $\dot{\gamma} > 0$, i.e., $2G\dot{\mathbf{e}}^{\mathrm{T}}\mathbf{X}^{\mathrm{S}} + \sqrt{2}\beta K X^{\mathrm{R}}\dot{\varepsilon}_{\mathrm{v}} > 0$.

3.1 Fully Explicit Updating Stress. The first proposed algorithm has a fully explicit character. For the Drucker–Prager plasticity, the algorithm was first devised by Liu [51] with no hardening and then developed for linear mixed hardening by the authors [36]. In this section, the scheme is advanced for the nonassociative plasticity of the same yield criterion but with generalized nonlinear kinematic hardening.

To update the stress, the dynamical system presented in Eq. (39) needs to be solved. Obviously, the augmented stress vector is time-dependent, which makes it too difficult to find a close solution of the system. Therefore, it is presumed for the control matrix to be independent of time. The result is a system of linear differential equations with constant coefficients and a close-form solution as follows:

$$\mathbf{X}(t) = \exp(\mathbb{A}t)\mathbf{X}(0) \tag{41}$$

where the initial conditions are

$$\mathbf{X}(0) = \begin{Bmatrix} \mathbf{X}_0^{\mathrm{S}} \\ X_0^{\mathrm{R}} \end{Bmatrix} = \begin{Bmatrix} \mathbf{s}'_0 \\ \sqrt{2}(\tau_{\mathrm{y},0} - \beta p'_0) \end{Bmatrix} \tag{42}$$

and, $\mathbf{s}'_0$ and p'_0 are the initial deviatoric and hydrostatic shifted stresses, respectively. To develop a numerical algorithm, a rectilinear strain-controlled route is adopted, which means that the $\dot{\mathbf{e}}$ and $\dot{\varepsilon}_{\mathrm{v}}$ are unvarying within each time step. It is also assumed that the radius of the yield surface and the back stress vector are constant through each time increment. Note that the yield-surface features, such as R and $\boldsymbol{\alpha}$, are not necessarily changeless during each load step, but in an explicit manner, they can be approximated by their values at the beginning of each time step. Based on these considerations, the coming solution to the dynamical system is expected

$$\mathbf{X}_{n+1} = \exp(\mathbb{A}_{n+\alpha}\Delta t)\mathbf{X}_{n+\alpha} = \mathbb{G}_{n+\alpha}\mathbf{X}_{n+\alpha} \tag{43}$$

where α separates the elastic and plastic parts of the load increment and is computed via Eq. (A3) as described in Appendix A. The subscript $n+\alpha$ means that the parameters are employed by their values on the elastic border. Hence, $\mathbf{X}_{n+\alpha}$ and $\mathbb{G}_{n+\alpha}$ are defined as follows:

$$\mathbf{X}_{n+\alpha} = \begin{Bmatrix} \mathbf{X}_{n+\alpha}^{\mathrm{S}} \\ X_{n+\alpha}^{\mathrm{R}} \end{Bmatrix} = \begin{Bmatrix} \mathbf{s}'_{n+\alpha}X_{n+1}^0 \\ R_{n+\alpha}X_{n+1}^0 \end{Bmatrix} \tag{44}$$

$$\mathbb{G}_{n+\alpha} = \begin{bmatrix} \mathbb{I}_{9\times 9} + (a_{n+\alpha} - 1)\Delta\hat{\boldsymbol{\mu}}\Delta\hat{\boldsymbol{\mu}}^{\mathrm{T}} & b_{n+\alpha}\Delta\hat{\boldsymbol{\mu}} \\ b_{n+\alpha}\Delta\hat{\boldsymbol{\mu}}^{\mathrm{T}} & a_{n+\alpha} \end{bmatrix}_{10\times 10} \tag{45}$$

The subsequent relationships are defined for $a_{n+\alpha}$, $b_{n+\alpha}$, and $\Delta\hat{\boldsymbol{\mu}}$

$$\Delta\hat{\boldsymbol{\mu}} = \frac{\Delta\boldsymbol{\mu}}{\|\Delta\boldsymbol{\mu}\|} \tag{46}$$

$$\Delta\boldsymbol{\mu} = (1-\alpha)\Delta\mathbf{e} + \frac{\lambda}{2G}\sum_{i=1}^{n} H_{\mathrm{nl},i}\boldsymbol{\alpha}_{n,i} \tag{47}$$

$$a_{n+\alpha} = \cosh\left(\frac{2G}{R_{n+\alpha}}\|\Delta\boldsymbol{\mu}\|\right) \tag{48}$$

$$b_{n+\alpha} = \sinh\left(\frac{2G}{R_{n+\alpha}}\|\Delta\boldsymbol{\mu}\|\right) \tag{49}$$

The discrete plastic multiplier, λ, also called the proportional factor, is calculated utilizing the next relationships

$$\lambda = (1-\alpha)\dot{\gamma}\Delta t = \frac{(1-\alpha)(2G\Delta\mathbf{e}^{\mathrm{T}}\mathbf{s}'_{n+\alpha} + 2\beta K(\tau_{\mathrm{y},0} - \beta p'_{n+\alpha})\Delta\varepsilon_{\mathrm{v}})}{2\bar{G}R_{n+\alpha}^2 - \mathbf{s}'_{n+\alpha}{}^{\mathrm{T}}\sum_{i=1}^{m} H_{\mathrm{nl},i}\boldsymbol{\alpha}_{n,i}} \tag{50}$$

$$\mathbf{s}'_{n+\alpha} = \mathbf{s}'_n + 2G\alpha\Delta\mathbf{e} \tag{51}$$

$$p'_{n+\alpha} = p'_n + \alpha K\Delta\varepsilon_v \tag{52}$$

$$R_{n+\alpha} = \sqrt{2}(\tau_{y,0} - \beta p'_{n+\alpha}) \tag{53}$$

Downloaded From: http://materialstechnology.asmedigitalcollection.asme.org/ on 05/25/2013 Terms of Use: http://asme.org/terms

In this investigation, $\Delta\mathbf{e}$ and $\Delta\varepsilon_v$ represent the deviatoric and volumetric portions of the nth strain increment. To obtain the updated augmented stress, $\mathbf{X}_{n+1}$, the relationships (43)–(45) can be utilized to solve the system of the differential equations in Eq. (39). Due to incompressible plastic deformation, the hydrostatic shifted stress is readily updated by the subsequent relationship, likewise yield-surface radius

$$p'_{n+1} = p'_{n+\alpha} + (1-\alpha)K\Delta\varepsilon_v \tag{54}$$

$$R_{n+1} = \sqrt{2}(\tau_{y,0} - \beta p'_{n+1}) \tag{55}$$

Having X^{R}_{n+1} and R_{n+1}, the integrating factor X^0_{n+1} has the below appearance

$$X^0_{n+1} = \frac{X^{\mathrm{R}}_{n+1}}{R_{n+1}} \tag{56}$$

Finally, after computing $\mathbf{X}^{\mathrm{S}}_{n+1}$ and X^0_{n+1} from the prior steps, the stress is updated, as follows:

$$\mathbf{s}'_{n+1} = \frac{\mathbf{X}^{\mathrm{S}}_{n+1}}{X^0_{n+1}} \tag{57}$$

What was acquired thus far was actually the updated deviatoric shifted stress, $\mathbf{s}'$, which sometimes it was called deviatoric stress or stress for short. However, the main goal is to update the deviatoric stress, $\mathbf{s}$. Evidently, the back stress vector stands between these two, which justifies the obligation to update the center of the yield surface. The following relationship cites the story:

$$\mathbf{s}_{n+1} = \mathbf{s}'_{n+1} + \boldsymbol{\alpha}_{n+1} \tag{58}$$

where $\mathbf{s}_{n+1}$ and $\boldsymbol{\alpha}_{n+1}$ have the below forms

$$\mathbf{s}_{n+1} = \mathbf{s}_n + 2G(\Delta\mathbf{e} - \Delta\mathbf{e}^{\mathrm{p}}) \tag{59}$$

$$\boldsymbol{\alpha}_{n+1} = \sum_{i=1}^{m}\boldsymbol{\alpha}_{n+1,i} = \sum_{i=1}^{m}\boldsymbol{\alpha}_{n,i} + \sum_{i=1}^{m}H_{\mathrm{kin},i}\Delta\mathbf{e}^{\mathrm{p}} - \lambda\sum_{i=1}^{m}H_{\mathrm{nl},i}\boldsymbol{\alpha}_{n,i} \tag{60}$$

It should be noted that the Equality (60) is achieved by integrating Eq. (18) from t_n to t_{n+1} and also estimating the $\boldsymbol{\alpha}$ by its value at the outset of the load step, $\boldsymbol{\alpha}_n$, which is a rational assumption since an explicit manner is being used. To achieve $\mathbf{s}_{n+1}$, the only unknown parameter is $\Delta\mathbf{e}^{\mathrm{p}}$. Using Eq. (13), the plastic part of the strain increment is attained, as follows:

$$\Delta\mathbf{e}^{\mathrm{p}} = \lambda\mathbf{s}'_{n+\alpha} \tag{61}$$

The proportional factor is easily computed from Eq. (33) through succeeding formula

$$\lambda = \frac{1}{2G}\ln(X^0_{n+1}) \tag{62}$$

Substituting λ in Eq. (61) with the former equation leads to the next relationship for $\Delta\mathbf{e}^{\mathrm{p}}$

$$\Delta\mathbf{e}^{\mathrm{p}} = \frac{1}{2G}\ln(X^0_{n+1})\mathbf{s}'_{n+\alpha} \tag{63}$$

Another approach to update the center of the yield surface is the reverse tactic, which means replacing the $\mathbf{s}_{n+1}$ and $\boldsymbol{\alpha}_{n+1}$ in Equality (58) with their equivalents from Eqs. (59) and (60) alongside using the Equality (62) for λ. This way leads to the following relationship for the plastic part of the deviatoric strain increment:

$$\Delta\mathbf{e}^{\mathrm{p}} = \frac{1}{2G}(\mathbf{s}_n + 2G\Delta\mathbf{e} - \bar{\mathbf{a}} - \mathbf{s}'_{n+1}) \tag{64}$$

The factor $\bar{\mathbf{a}}$ is also determined from the below relation

$$\bar{\mathbf{a}} = \sum_{i=1}^{m}\boldsymbol{\alpha}_{n,i}\left(1 - \frac{H_{\mathrm{nl},i}}{2G}\ln(X^0_{n+1})\right) \tag{65}$$

3.2 Semi Implicit Updating Stress. In the previous technique, fully explicit, the characteristics of the yield surface were estimated by their values at the beginning of each time increment to solve the dynamical system in spite of being varied. Obviously, this seems a bit rough approximation where better ones could be taken. Thus, the authors decided to develop a numerical algorithm which is capable of utilizing better approximations of the yield-surface features. To reach the goal, another exponential-based integration is utilized. It is called semi-implicit since it uses the unknown features of the yield surface. The scheme was first devised by Rezaiee Pajand and Nasirai [57] and was developed for a Drucker–Prager plasticity with no hardening. Here the scheme is progressed for the nonlinear kinematic hardening. In accordance with the strategy, the values of R and $\boldsymbol{\alpha}$ at the middle of each time increment are hired to gain better responses rather than R_n and $\boldsymbol{\alpha}_n$. It is expected that the greater estimations of R and $\boldsymbol{\alpha}$ will enhance the accuracy and convergence of the numerical approach.

Considering that the back stress vector, $\boldsymbol{\alpha}$, and the value of the yield-surface radius, R, could be chosen in an arbitrary point of the load step and it might be a subject of debate, the numerical algorithm is derived in a broad form using parameter ξ. This factor denotes a specified point of each load increment, $0 < \xi < 1$. For example, the subscript $n+\xi(1-\alpha)$ alongside assuming $\xi = 0.5$, denotes the amount of the intended parameter at the middle point of the plastic part of the n*th* load increment. Taking a rectilinear strain-controlled path and aforementioned procedure for specifying $\boldsymbol{\alpha}$ and R, the augmented stress vector at time t_{n+1} is updated by a two-step procedure.

At the first step, the deviatoric shifted stress, $\mathbf{s}'$, back stress vector, $\boldsymbol{\alpha}$, and the radius of the yield surface, R, are computed at the specified point, which is denoted by $n+\xi(1-\alpha)$, using their values on the yield surface, $\mathbf{s}'_{n+\alpha}$, $\boldsymbol{\alpha}_{n+\alpha}$ and $R_{n+\alpha}$. Again, the whole process is carried out at the second step, but this time by hiring the computed stress, $\mathbf{s}'_{n+\xi(1-\alpha)}$, and the features of the yield surface, $\boldsymbol{\alpha}_{n+\xi(1-\alpha)}$ and $R_{n+\xi(1-\alpha)}$, from the previous step. This process leads to the updated deviatoric and back stresses at the end of the load increment, $\mathbf{s}'_{n+1}$ and $\boldsymbol{\alpha}_{n+1}$. In the subsequent parts, the required mathematical formulas of the aforementioned methodology will come.

3.2.1 Step One. The system of the differential equations is changed at the first step to the below form

$$\mathbf{X}_{n+\xi(1-\alpha)} = \exp(\mathbb{A}^{\xi}_{n+\alpha}\Delta t)\mathbf{X}_{n+\alpha} = \mathbb{G}^{\xi}_{n+\alpha}\mathbf{X}_{n+\alpha} \tag{66}$$

In this relation, $\mathbb{G}^{\xi}_{n+\alpha}$ is the exponential matrix of the dynamical system. At each plastic load increment, this matrix is specified at point ξ, as follows:

$$\mathbb{G}^{\xi}_{n+\alpha} = \begin{bmatrix} \mathbb{I}_{9\times 9} + (a^{\xi}_{n+\alpha} - 1)\Delta\hat{\boldsymbol{\mu}}^{\xi}_{n+\alpha}\Delta\hat{\boldsymbol{\mu}}^{\xi\mathrm{T}}_{n+\alpha} & b^{\xi}_{n+\alpha}\Delta\hat{\boldsymbol{\mu}}^{\xi}_{n+\alpha} \\ b^{\xi}_{n+\alpha}\Delta\hat{\boldsymbol{\mu}}^{\xi\mathrm{T}}_{n+\alpha} & a^{\xi}_{n+\alpha} \end{bmatrix}_{10\times 10} \tag{67}$$

The scalars $a^{\xi}_{n+\alpha}$, $b^{\xi}_{n+\alpha}$ and the vector $\Delta\hat{\boldsymbol{\mu}}^{\xi}_{n+\alpha}$ are obtained by the next relationships

$$\Delta\hat{\boldsymbol{\mu}}^{\xi}_{n+\alpha} = \frac{\Delta\boldsymbol{\mu}^{\xi}_{n+\alpha}}{\left\|\Delta\boldsymbol{\mu}^{\xi}_{n+\alpha}\right\|} \tag{68}$$

$$\Delta\boldsymbol{\mu}^{\xi}_{n+\alpha} = \xi(1-\alpha)\Delta\mathbf{e} + \frac{\lambda^{\xi}_{n+\alpha}}{2G}\sum_{i=1}^{m}H_{\mathrm{nl},i}\boldsymbol{\alpha}_{n,i} \tag{69}$$

Downloaded From: http://materialstechnology.asmedigitalcollection.asme.org/ on 05/25/2013 Terms of Use: http://asme.org/terms

$$\lambda^{\xi}_{n+\alpha} = \xi(1-\alpha)\dot{\gamma}\Delta t = \frac{\xi(1-\alpha)(2G\Delta\mathbf{e}^{\mathrm{T}}\mathbf{s}'_{n+\alpha} + 2\beta K(\tau_y - \beta p'_{n+\alpha})\Delta\varepsilon_{\mathrm{v}})}{2\bar{G}R^2_{n+\alpha} - \mathbf{s}'^{\mathrm{T}}_{n+\alpha}\sum_{i=1}^{m} H_{\mathrm{nl},i}\boldsymbol{\alpha}_{n,i}} \tag{70}$$

$$\begin{aligned} a^{\xi}_{n+\alpha} &= \cosh\left(\frac{2G}{R_{n+\alpha}}||\Delta\boldsymbol{\mu}^{\xi}_{n+\alpha}||\right) \\ b^{\xi}_{n+\alpha} &= \sinh\left(\frac{2G}{R_{n+\alpha}}||\Delta\boldsymbol{\mu}^{\xi}_{n+\alpha}||\right) \end{aligned} \tag{71}$$

where $\mathbf{s}'_{n+\alpha}$, $p'_{n+\alpha}$, and $R_{n+\alpha}$ are calculated by Eqs. (51)–(53). The rest of the first step is the same as the technique described in the fully explicit updating method. In the following lines, the process will be briefly presented to avoid any confusion. The yield-surface radius and the volumetric shifted stress are calculated at the end of the first step by next equalities

$$R_{n+\xi(1-\alpha)} = \sqrt{2}(\tau_y - \beta p'_{n+\xi(1-\alpha)}) \tag{72}$$

$$p'_{n+\xi(1-\alpha)} = p'_{n+\alpha} + \xi(1-\alpha)K\Delta\varepsilon_{\mathrm{v}} \tag{73}$$

Having solved the system of equations in Eq. (66) and acquiring $\mathbf{X}^{\mathrm{S}}_{n+\xi(1-\alpha)}$ and $X^{\mathrm{R}}_{n+\xi(1-\alpha)}$, the deviatoric stress is obtained at the specified point of $n+\xi(1-\alpha)$, as follows:

$$X^0_{n+\xi(1-\alpha)} = \frac{X^{\mathrm{R}}_{n+\xi(1-\alpha)}}{R_{n+\xi(1-\alpha)}} \rightarrow \mathbf{s}'_{n+\xi(1-\alpha)} = \frac{\mathbf{X}^{\mathrm{S}}_{n+\xi(1-\alpha)}}{X^0_{n+\xi(1-\alpha)}} \tag{74}$$

It is also needed to attain the back stress vector at the point of $n+\xi(1-\alpha)$, so it will be used in the next step. Utilizing the same approach as discussed previously, the center of the yield surface is updated through the coming relationship

$$\boldsymbol{\alpha}_{n+\xi(1-\alpha)} = \sum_{i=1}^{m}\boldsymbol{\alpha}_{n+\xi(1-\alpha),i} = \sum_{i=1}^{m}\bar{\mathbf{a}}_i + \sum_{i=1}^{m}\bar{H}_i\Delta\mathbf{e}^{\mathrm{p}}_{n+\xi(1-\alpha)} \tag{75}$$

where $\bar{\mathbf{a}}_i$ and $\bar{H}_i$ are defined as

$$\bar{\mathbf{a}}_{n,i} = \left(\frac{1 - \frac{H_{\mathrm{nl},i}}{4\bar{G}}\ln(X^0_{n+\xi(1-\alpha)})}{1 + \frac{H_{\mathrm{nl},i}}{4\bar{G}}\ln(X^0_{n+\xi(1-\alpha)})}\right)\boldsymbol{\alpha}_{n,i} \tag{76}$$

$$\bar{H}_i = \frac{H_{\mathrm{kin},i}}{1 + \frac{H_{\mathrm{nl},i}}{4\bar{G}}\ln(X^0_{n+\xi(1-\alpha)})} \tag{77}$$

Using the same strategy as explained in Sec. 3.1, the plastic strain deviator is attained employing Eqs. (58), (59), and (75)–(77) with the below shape

$$\Delta\mathbf{e}^{\mathrm{p}}_{n+\xi(1-\alpha)} = \frac{1}{2G + \sum_{i=1}^{m}\bar{H}_i}\left(\mathbf{s}_n + G\Delta\mathbf{e} - \sum_{i=1}^{m}\bar{\mathbf{a}}_i - \mathbf{s}'_{n+\xi(1-\alpha)}\right) \tag{78}$$

3.2.2 *Step Two*. The whole process will be recurred at the second step except for the fact that, at this time, the deviatoric stress and the features of the yield surface acquired from the preceding step are used. The coming words and relationships thoroughly explain it

$$\mathbf{X}_{n+1} = \exp(\mathbb{A}_{n+\xi(1-\alpha)}\Delta t)\mathbf{X}_{n+\alpha} = \mathbb{G}_{n+\xi(1-\alpha)}\mathbf{X}_{n+\alpha} \tag{79}$$

The vectors $\mathbf{X}_{n+1}$ and $\mathbf{X}_{n+\alpha}$ have the next appearances

$$\mathbf{X}_{n+1} = \begin{Bmatrix} \mathbf{X}^{\mathrm{s}}_{n+1} \\ X^{\mathrm{R}}_{n+1} \end{Bmatrix} = \begin{Bmatrix} \mathbf{s}'_{n+1}X^0_{n+1} \\ R_{n+1}X^0_{n+1} \end{Bmatrix}, \quad \mathbf{X}_{n+\alpha} = \begin{Bmatrix} \mathbf{X}^{\mathrm{S}}_{n+\alpha} \\ X^{\mathrm{R}}_{n+\alpha} \end{Bmatrix} = \begin{Bmatrix} \mathbf{s}'_{n+\alpha}X^0_{n+\alpha} \\ R_{n+\alpha}X^0_{n+\alpha} \end{Bmatrix} \tag{80}$$

As it is seen, the factor matrix, $\mathbb{G}_{n+\xi(1-\alpha)}$, is attained using the termination point of the previous step. It is formed in the below shape

$$\mathbb{G}_{n+\xi(1-\alpha)} = \begin{bmatrix} \mathbb{I}_{9\times 9} + (a_{n+\xi(1-\alpha)} - 1)\Delta\hat{\boldsymbol{\mu}}_{n+\xi(1-\alpha)}\Delta\hat{\boldsymbol{\mu}}^{\mathrm{T}}_{n+\xi(1-\alpha)} & b_{n+\xi(1-\alpha)}\Delta\hat{\boldsymbol{\mu}}_{n+\xi(1-\alpha)} \\ b_{n+\xi(1-\alpha)}\Delta\hat{\boldsymbol{\mu}}^{\mathrm{T}}_{n+\xi(1-\alpha)} & a_{n+\xi(1-\alpha)} \end{bmatrix}_{10\times 10} \tag{81}$$

where the parameters $a_{n+\xi(1-\alpha)}$, $b_{n+\xi(1-\alpha)}$, and $\Delta\hat{\boldsymbol{\mu}}_{n+\xi(1-\alpha)}$ are obtained by the next relationships

$$\Delta\hat{\boldsymbol{\mu}}_{n+\xi(1-\alpha)} = \frac{\Delta\boldsymbol{\mu}_{n+\xi(1-\alpha)}}{\left\|\Delta\boldsymbol{\mu}_{n+\xi(1-\alpha)}\right\|} \tag{82}$$

$$\Delta\boldsymbol{\mu}_{n+\xi(1-\alpha)} = (1-\alpha)\Delta\mathbf{e} + \frac{\lambda_{n+\xi(1-\alpha)}}{2G}\sum_{i=1}^{m}H_{\mathrm{nl},i}\boldsymbol{\alpha}_{n+\xi(1-\alpha),i} \tag{83}$$

The proportional factor $\lambda_{n+\xi(1-\alpha)}$ is calculated by the subsequent equation

$$\lambda_{n+\xi(1-\alpha)} = (1-\alpha)\dot{\gamma}\Delta t = \frac{(1-\alpha)(2G\Delta\mathbf{e}^{\mathrm{T}}\mathbf{s}'_{n+\xi(1-\alpha)} + 2\beta K(\tau_y - \beta p'_{n+\xi(1-\alpha)})\Delta\varepsilon_{\mathrm{v}})}{2\bar{G}R^2_{n+\xi(1-\alpha)} - \mathbf{s}'_{n+\xi(1-\alpha)}{}^{\mathrm{T}}\sum_{i=1}^{m}H_{\mathrm{nl},i}\boldsymbol{\alpha}_{n+\xi(1-\alpha),i}} \tag{84}$$

$$\begin{aligned} a_{n+\xi(1-\alpha)} &= \cosh\left(\frac{2G}{R_{n+\xi(1-\alpha)}}||\Delta\boldsymbol{\mu}_{n+\xi(1-\alpha)}||\right) \\ b_{n+\xi(1-\alpha)} &= \sinh\left(\frac{2G}{R_{n+\xi(1-\alpha)}}||\Delta\boldsymbol{\mu}_{n+\xi(1-\alpha)}||\right) \end{aligned} \tag{85}$$

Having resolved the system of the differential equations and attaining $\mathbf{X}^{\mathrm{S}}_{n+1}$ and X^{R}_{n+1}, one can update the deviatoric shifted stress at the end of the load step, $\mathbf{s}'_{n+1}$, using Eqs. (55)–(57). Updating the deviatoric stress, $\mathbf{s}_{n+1}$, requires that the new position of the yield-surface center be specified, which is designated by the back stress vector, $\boldsymbol{\alpha}_{n+1}$. It is achieved by integrating the equalities (17) and (18) on the whole load interval

$$\boldsymbol{\alpha}_{n+1} - \boldsymbol{\alpha}_n = \sum_{i=1}^{m}\int_{t_n}^{t_{n+1}} H_{\mathrm{kin},i}\dot{\mathbf{e}}^{\mathrm{p}} - H_{\mathrm{nl},i}\dot{\gamma}\boldsymbol{\alpha}_i dt \tag{86}$$

Due to the fact that $H_{\mathrm{kin},i}$ and $H_{\mathrm{nl},i}$ are constant during each load increment, $\boldsymbol{\alpha}_i$ should be estimated by a constant vector within

Downloaded From: http://materialstechnology.asmedigitalcollection.asme.org/ on 05/25/2013 Terms of Use: http://asme.org/terms

each load step to integrate the previous equation. It is usual for the back stress to be estimated at the beginning of each load step, particularly in the explicit manners, which is not a good appraisal. Therefore, exchanging it with the previously obtained vector from the first step, $\boldsymbol{\alpha}_{n+\xi(1-\alpha),i}$, will generate better and more dependable results owing to more accurate approximation for $\boldsymbol{\alpha}_i$. Hence, the center of the yield surface is updated through the next equality

$$\boldsymbol{\alpha}_{n+1} = \sum_{i=1}^{m} \boldsymbol{\alpha}_{n+1,i} = \sum_{i=1}^{m} \boldsymbol{\alpha}_{\mathrm{n},i} + \sum_{i=1}^{m} H_{\mathrm{kin},i}\Delta\mathbf{e}^{\mathrm{p}} - \lambda_{n+\xi(1-\alpha)} \times \sum_{i=1}^{m} H_{\mathrm{nl},i}\boldsymbol{\alpha}_{n+\xi(1-\alpha),i} \tag{87}$$

The last equation along with Eqs. (58), (59), and (62) give rise to Eq. (64) for $\Delta\mathbf{e}^{\mathrm{p}}$ with the exception of $\bar{\mathbf{a}}$ from the next equality

$$\bar{\mathbf{a}} = \sum_{i=1}^{m} \left(\boldsymbol{\alpha}_{n,i} - \frac{H_{\mathrm{nl},i}}{2\bar{G}} \ln(X^{0}_{n+1})\boldsymbol{\alpha}_{n+\xi(1-\alpha),i} \right) \tag{88}$$

One can also choose the simple direct way to obtain the $\Delta\mathbf{e}^{\mathrm{p}}$ which is, of course, accompanied with lower accuracy and performance. This approach gives the below result

$$\Delta\mathbf{e}^{\mathrm{p}} = \frac{1}{2\bar{G}} \ln(X^{0}_{n+1})\mathbf{s}'_{n+\xi(1-\alpha)} \tag{89}$$

To sum up, the aforementioned technique for stress updating comes with superior accuracy and better convergence rate since it virtually merges two steps in one. It actually uses better estimations of $\boldsymbol{\alpha}$, R, and $\mathbf{s}'$ in the incremental pace of the numerical algorithm to acquire the desired parameters, $\mathbf{s}'_{n+1}$ and $\mathbf{s}_{n+1}$. Furthermore, it will increase the performance by means of declining the computational time alongside more accurate responses. It is also worth mentioning that in all the numerical tests to come, the parameter ξ is adopted 0.5 for being a logical choice taking the values at the middle of each load step. Figure 1 presents a general flow chart for the both proposed schemes to better perceive them.

4 Treatment of the Apex

There is a sharp point at the tip of the Drucker–Prager's cone called apex. This causes a singularity in the yield-surface function. In order for it to cope, it is conventional to define a complementary cone working as an indicator to show whether the trial stress is placed inside the area of the apex influence or not [36,60]. For an associative plasticity model, this cone is postulated with its flank orthogonal to those of the convex set, considering that the plastic strain flow is defined via the subdifferential of the indicator function of the yield surface, see Fig. 2. For the assumed nonassociative plasticity model, the plastic strain flow is not orthogonal to the loading surface. In contrast, it is perpendicular to the hydrostatic pressure axis, since the von-Mises yield function

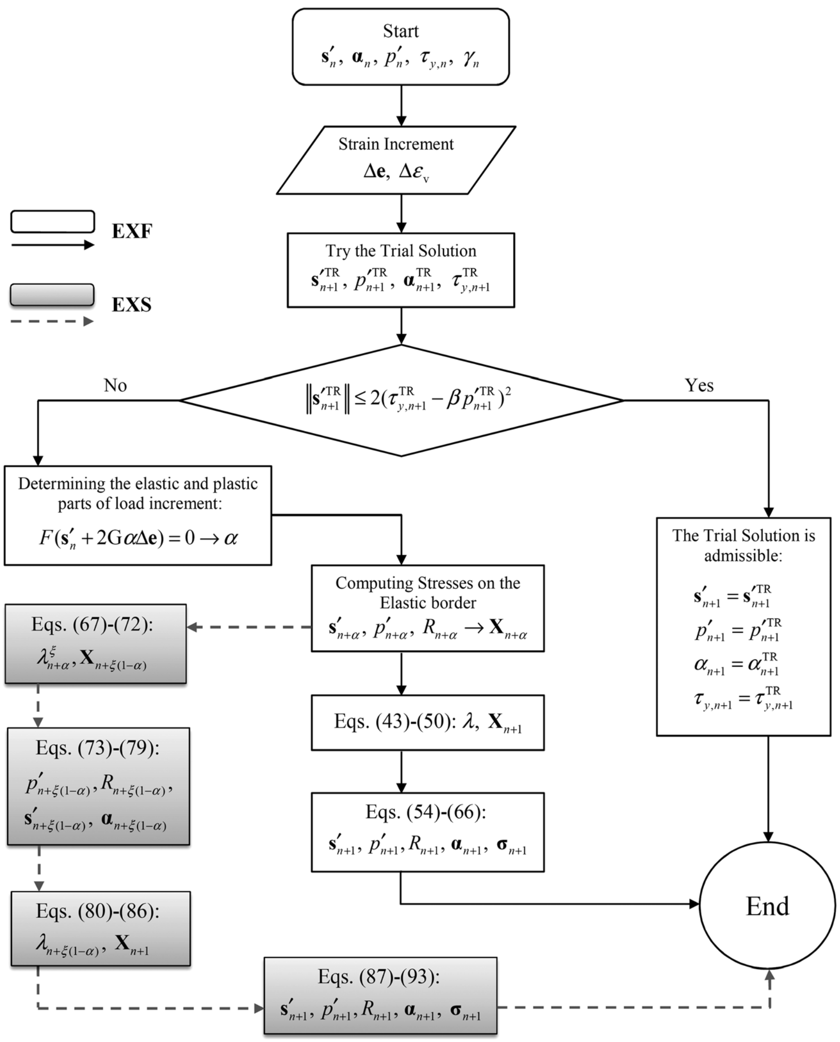

Fig. 1 Flow chart for the explicit exponential, EXF, and semi-implicit exponential, EXS, integrations

Downloaded From: http://materialstechnology.asmedigitalcollection.asme.org/ on 05/25/2013 Terms of Use: http://asme.org/terms

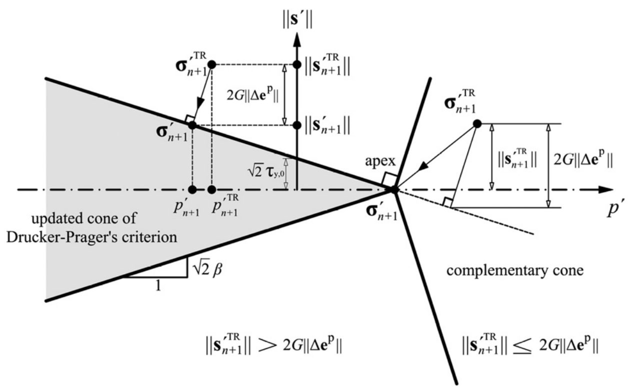

Fig. 2 Treatment of the apex for associative model

has been taken in its flow rule. Therefore, the complementary cone's flank should be upright as in Fig. 3.

In overall, the stress-updating process would follow its routine method preceded before if the trial stress was situated outside of the complementary cone; otherwise, the $\boldsymbol{\sigma}'^{\mathrm{TR}}_{n+1}$ would be in the realm of the apex influence which suggests that the trial stress must fall back to the apex.

(1) The updated stress lies on the smooth portion of the cone, i.e., $||\mathbf{s}'^{\mathrm{TR}}_{n+1}|| > 2G||\Delta\mathbf{e}^{\mathrm{p}}||$
(2) The updated stress settles on the apex of the cone, i.e., $||\mathbf{s}'^{\mathrm{TR}}_{n+1}|| \leq 2G||\Delta\mathbf{e}^{\mathrm{p}}||$

For the first state, the process of updating stress was presented in Secs. 3.1 and 3.2. What appears later is the procedure that should be taken to update the stress in the event of the second condition

$$\mathbf{s}'_{n+1} = 0 \tag{90}$$

$$R_{n+1} = \sqrt{2}(\tau_{\mathrm{y},0} - \beta p'_{n+1}) = 0 \rightarrow p'_{n+1} = \frac{\tau_{\mathrm{y},0}}{\beta} \tag{91}$$

After the deviatoric and hydrostatic shifted stresses were updated, the back stress vector must be updated to acquire the deviatoric stress, $\mathbf{s}_{n+1}$. Considering Eq. (20), the following relationship is attained:

$$\mathbf{s}'_{n+1} - \mathbf{s}'_n = 2G\Delta\mathbf{e}^{\mathrm{e}} - \sum_{i=1}^{m} H_{\mathrm{kin},i}\Delta\mathbf{e}^{\mathrm{p}} + \lambda \sum_{i=1}^{m} H_{\mathrm{nl},i}\boldsymbol{\alpha}_{n,i} \tag{92}$$

Evidently, updating the back stress vector means computing $\Delta\mathbf{e}^{\mathrm{p}}$, which concerns the rest of the operation. Employing Eqs. (7) and (92) and the subsequent equation to substitute for λ

$$\lambda = \frac{2G\Delta\mathbf{e}^{\mathrm{T}}\mathbf{s}'_n + 2\beta K(\tau_{\mathrm{y},0} - \beta p'_n)\Delta\varepsilon_{\mathrm{v}}}{2\bar{G}R_n^2 - \mathbf{s}'^{\mathrm{T}}_n \sum_{i=1}^{m} H_{\mathrm{nl},i}\boldsymbol{\alpha}_{n,i}} \tag{93}$$

leads to the following equality:

$$2G\Delta\mathbf{e} + \mathbf{s}'_n = 2\bar{G}\Delta\mathbf{e}^{\mathrm{p}} - \lambda \sum_{i=1}^{m} H_{\mathrm{nl},i}\boldsymbol{\alpha}_{n,i} \tag{94}$$

The left side of the former equation can be replaced with the next relationship

$$\mathbf{s}^{\mathrm{TR}}_{n+1} - \boldsymbol{\alpha}_n = 2G\Delta\mathbf{e} + \mathbf{s}'_n \tag{95}$$

Therefore, the plastic part of the strain increment is obtained by the below formula

$$\Delta\mathbf{e}^{\mathrm{p}} = \frac{1}{2\bar{G}}\left(\mathbf{s}^{\mathrm{TR}}_{n+1} - \boldsymbol{\alpha}_n + \lambda \sum_{i=1}^{m} H_{\mathrm{nl},i}\alpha_{n,i}\right) \tag{96}$$

5 Consistent Tangent Modulus

Through the Newton–Raphson algorithm, the tangent modulus, which is consistent with the integration scheme, is essential for achieving the asymptotic quadratic convergence rate in a finite-element analysis. In the following lines, the tangent operators are derived for the proposed integration schemes, fully explicit exponential map (EXF) and semi-implicit exponential map (EXS), as well as the forward Euler and backward Euler techniques. As displayed in Appendix C, the general relationship of the tangent operator is attained departing the deviatoric and volumetric parts of the stress

$$\frac{\partial \boldsymbol{\sigma}_{n+1}}{\partial \varepsilon_{n+1}} = \left(\frac{\partial \mathbf{s}'_{n+1}}{\partial \mathbf{e}_{n+1}} + \frac{\partial \boldsymbol{\alpha}_{n+1}}{\partial \mathbf{e}_{n+1}}\right)\mathbb{I}_{\mathrm{dev}} + K(\mathbf{i}\mathbf{i}^{\mathrm{T}}) \tag{97}$$

5.1 Forward Euler Consistent Tangent Modulus. Referring to Eq. (97), the derivatives $\partial\mathbf{s}'_{n+1}/\partial\mathbf{e}_{n+1}$ and $\partial\boldsymbol{\alpha}_{n+1}/\partial\mathbf{e}_{n+1}$ must be calculated. If $\mathbf{s}''$ represents the deviatoric shifted stress prior to implementing the correcting vector, $a_{\mathrm{f}}\mathbf{n}_{n+1}$, the adjusted deviatoric shifted stress, $\mathbf{s}'$, will be computed by the below formulas

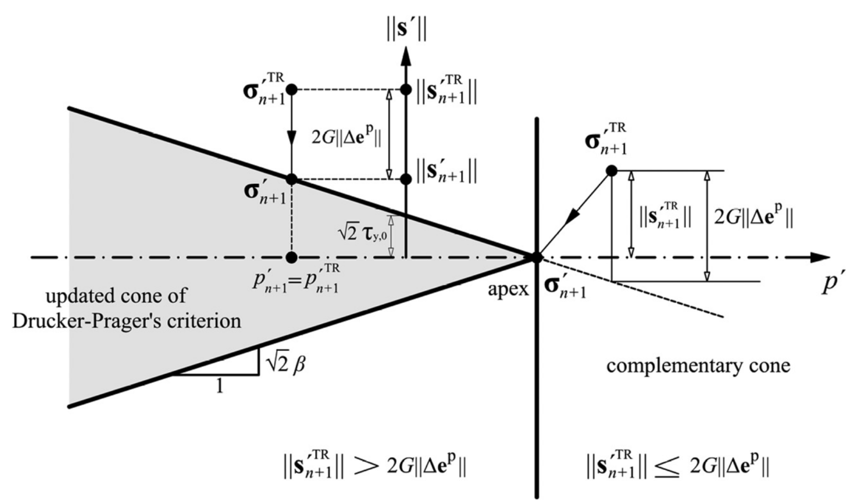

Fig. 3 Treatment of the apex for nonassociative model

Downloaded From: http://materialstechnology.asmedigitalcollection.asme.org/ on 05/25/2013 Terms of Use: http://asme.org/terms

$$\mathbf{s}'_{n+1} = \mathbf{s}''_{n+1} + a_f \mathbf{n}_{n+1}, \quad \mathbf{n}_{n+1} = \frac{\mathbf{s}''_{n+1}}{\|\mathbf{s}''_{n+1}\|} \tag{98}$$

Taking the derivative of the previous equation with respect to $\mathbf{e}_{n+1}$ leads to the next result

$$\frac{\partial \mathbf{s}'_{n+1}}{\partial \mathbf{e}_{n+1}} = \frac{\partial \mathbf{s}''_{n+1}}{\partial \mathbf{e}_{n+1}} + \frac{\partial a_f}{\partial \mathbf{e}_{n+1}} \mathbf{n}^{\mathrm{T}}_{n+1} + a_f \frac{\partial \mathbf{n}_{n+1}}{\partial \mathbf{e}_{n+1}} \tag{99}$$

Using Eqs. (A6), (A10), and (A11), the constituents of $\partial \mathbf{s}'_{n+1}/\partial \mathbf{e}_{n+1}$ are computed, as follows:

$$\frac{\partial \mathbf{s}''_{n+1}}{\partial \mathbf{e}_{n+1}} = 2G(1-\alpha)\mathbb{I}_{\mathrm{dev}} + (1 - 2\bar{G}\lambda)\frac{\partial \mathbf{s}'_{n+\alpha}}{\partial \mathbf{e}_{n+1}} - 2G\frac{\partial \alpha}{\partial \mathbf{e}_{n+1}}\Delta\mathbf{e}^{\mathrm{T}} + \left(\sum_{i=1}^{m} H_{\mathrm{nl},i}\boldsymbol{\alpha}_{n,i} - 2\bar{G}\mathbf{s}'_{n+\alpha}\right)\frac{\partial \lambda^{\mathrm{T}}}{\partial \mathbf{e}_{n+1}} \tag{100}$$

where the derivatives of $\mathbf{s}'_{n+\alpha}$, α, and λ are presented in Appendix D. $\partial \mathbf{n}_{n+1}/\partial \mathbf{e}_{n+1}$ and $\partial a_f/\partial \mathbf{e}_{n+1}$ are computed through the coming relationships

$$\frac{\partial \mathbf{n}_{n+1}}{\partial \mathbf{e}_{n+1}} = \frac{1}{\|\mathbf{s}''_{n+1}\|^2}\left(\frac{\partial \mathbf{s}''_{n+1}}{\partial \mathbf{e}_{n+1}}\|\mathbf{s}''_{n+1}\| - \frac{\partial \mathbf{s}''_{n+1}}{\partial \mathbf{e}_{n+1}}\frac{\mathbf{s}''_{n+1}{}^{\mathrm{T}}\mathbf{s}''_{n+1}}{\|\mathbf{s}''_{n+1}\|}\right) \tag{101}$$

in which $\partial \mathbf{s}''_{n+1}/\partial \mathbf{e}_{n+1}$ has been gained from the previous equality. The computed $\partial \mathbf{n}_{n+1}/\partial \mathbf{e}_{n+1}$ along with Eq. (A10) are utilized to obtain $\partial a_f/\partial \mathbf{e}_{n+1}$, as given below

$$\frac{\partial a_f}{\partial \mathbf{e}_{n+1}} = \frac{2(\mathbf{n}^{\mathrm{T}}_{n+1}\mathbf{s}''_{n+1})\left(\frac{\partial \mathbf{n}_{n+1}}{\partial \mathbf{e}_{n+1}}\mathbf{s}''_{n+1} + \frac{\partial \mathbf{s}''_{n+1}}{\partial \mathbf{e}_{n+1}}\mathbf{n}_{n+1}\right) - 2\frac{\partial \mathbf{s}''_{n+1}}{\partial \mathbf{e}_{n+1}}\mathbf{s}''_{n+1}}{2\sqrt{(\mathbf{n}^{\mathrm{T}}_{n+1}\mathbf{s}''_{n+1})^2 - \|\mathbf{s}''_{n+1}\|^2 + R^2_{n+1}}} - \left(\frac{\partial \mathbf{n}_{n+1}}{\partial \mathbf{e}_{n+1}}\mathbf{s}''_{n+1} + \frac{\partial \mathbf{s}''_{n+1}}{\partial \mathbf{e}_{n+1}}\mathbf{n}_{n+1}\right) \tag{102}$$

Having $\partial \mathbf{s}'_{n+1}/\partial \mathbf{e}_{n+1}$, the only remained part to calculate the tangent modulus from Eq. (97) is obtained by the next equality, which has been achieved using Eq. (A9)

$$\frac{\partial \boldsymbol{\alpha}_{n+1}}{\partial \mathbf{e}_{n+1}} = \sum_{i=1}^{m}\left(H_{\mathrm{kin},i}\left(\frac{\partial \lambda}{\partial \mathbf{e}_{n+1}}\mathbf{s}'_{n+\alpha} + \lambda\frac{\partial \mathbf{s}'_{n+\alpha}}{\partial \mathbf{e}_{n+1}}\right) - H_{\mathrm{nl},i}\frac{\partial \lambda}{\partial \mathbf{e}_{n+1}}\boldsymbol{\alpha}^{\mathrm{T}}_{n,i}\right) \tag{103}$$

5.2 Backward Euler Consistent Tangent Modulus. To formulate the consistent tangent modulus of the backward Euler algorithm for the considered plasticity, it requires that the derivatives of $\mathbf{s}'_{n+1}$ and $\boldsymbol{\alpha}_{n+1}$ with respect to $\mathbf{e}_{n+1}$ be found. Referring to Appendix B, one can hire Eq. (B1) to reach $\partial \mathbf{s}'_{n+1}/\partial \mathbf{e}_{n+1}$

$$\frac{\partial \mathbf{s}'_{n+1}}{\partial \mathbf{e}_{n+1}} = \frac{1}{1 + 2\bar{G}\lambda - \lambda^2 C_1}\left(\frac{\partial \mathbf{s}'^{\mathrm{TR}}_{n+1}}{\partial \mathbf{e}_{n+1}} + (-2\bar{G} + 2\lambda C_1 - \lambda^2 C_2)\frac{\partial \lambda}{\partial \mathbf{e}_{n+1}}\mathbf{s}'^{\mathrm{T}}_{n+1} + \frac{\partial \lambda}{\partial \mathbf{e}_{n+1}}(\mathbf{C}^{\mathrm{T}}_3 - \lambda\mathbf{C}^{\mathrm{T}}_4)\right) \tag{104}$$

For absence of complexity and ambiguity, the scalars C_1 and C_2 also the vectors $\mathbf{C}_3$ and $\mathbf{C}_4$ are defined in the following shapes:

$$C_1 = \sum_{i=1}^{m}\frac{H_{\mathrm{nl},i}H_{\mathrm{kin},i}}{1 + \lambda H_{\mathrm{nl},i}} \tag{105}$$

$$C_2 = \sum_{i=1}^{m}\frac{H^2_{\mathrm{nl},i}H_{\mathrm{kin},i}}{(1 + \lambda H_{\mathrm{nl},i})^2} \tag{106}$$

$$\mathbf{C}_3 = \sum_{i=1}^{m}\frac{H_{\mathrm{nl},i}}{1 + \lambda H_{\mathrm{nl},i}}\boldsymbol{\alpha}_{n,i} \tag{107}$$

$$\mathbf{C}_4 = \sum_{i=1}^{m}\frac{H^2_{\mathrm{nl},i}}{(1 + \lambda H_{\mathrm{nl},i})^2}\boldsymbol{\alpha}_{n,i} \tag{108}$$

To differentiate $\boldsymbol{\alpha}_{n+1}$ with respect to $\mathbf{e}_{n+1}$, Eq. (B3) will be utilized, which eventually leads to the succeeding results

$$\frac{\partial \boldsymbol{\alpha}_{n+1}}{\partial \mathbf{e}_{n+1}} = \sum_{i=1}^{m}\frac{\partial \boldsymbol{\alpha}_{n+1,i}}{\partial \mathbf{e}_{n+1}} \tag{109}$$

$$\frac{\partial \boldsymbol{\alpha}_{n+1,i}}{\partial \mathbf{e}_{n+1}} = \frac{H_{\mathrm{kin},i}}{1 + H_{\mathrm{nl},i}\lambda}\left(\frac{\partial \lambda}{\partial \mathbf{e}_{n+1}}\mathbf{s}'_{n+1}{}^{\mathrm{T}} + \lambda\frac{\partial \mathbf{s}'_{n+1}}{\partial \mathbf{e}_{n+1}}\right) - \frac{H_{\mathrm{kin},i}H_{\mathrm{nl},i}}{(1 + H_{\mathrm{nl},i}\lambda)^2}\frac{\partial \lambda}{\partial \mathbf{e}_{n+1}}\left(\frac{1}{H_{\mathrm{kin},i}}\boldsymbol{\alpha}_{n,i}{}^{\mathrm{T}} + \lambda\mathbf{s}'^{\mathrm{T}}_{n+1}\right) \tag{110}$$

As it is perceived from the former relationships, calculating $\partial \mathbf{s}'_{n+1}/\partial \mathbf{e}_{n+1}$ and $\partial \boldsymbol{\alpha}_{n+1}/\partial \mathbf{e}_{n+1}$ is contingent on coming by the derivative of the proportional factor with regards to $\mathbf{e}_{n+1}$ that will be managed using Eq. (B5). The below relationship for $\partial \lambda/\partial \mathbf{e}_{n+1}$ is the outcome of differentiating the aforementioned equality with respect to $\mathbf{e}_{n+1}$

$$\frac{\partial \lambda}{\partial \mathbf{e}_{n+1}} = \frac{\frac{\partial \mathbf{s}'^{\mathrm{TR}}_{n+1}}{\partial \mathbf{e}_{n+1}}(\mathbf{s}'^{\mathrm{TR}}_{n+1} + \lambda\mathbf{C}_3)}{\frac{\|\mathbf{s}'^{\mathrm{TR}}_{n+1} + \lambda\mathbf{C}_3\|^2}{(1 + 2\bar{G}\lambda - \lambda^2 C_1)}(2\bar{G} - 2\lambda C_1 + \lambda^2 C_2) - (\mathbf{C}_3 - \lambda\mathbf{C}_4)^{\mathrm{T}}(\mathbf{s}'^{\mathrm{TR}}_{n+1} + \lambda\mathbf{C}_3)} \tag{111}$$

5.3 Fully Explicit Exponential Consistent Tangent Modulus. Considering Eq. (97), $\partial \boldsymbol{\sigma}_{n+1}/\partial \mathbf{e}_{n+1}$ is achieved calculating $\partial \mathbf{s}'_{n+1}/\partial \mathbf{e}_{n+1}$ and $\partial \boldsymbol{\alpha}_{n+1}/\partial \mathbf{e}_{n+1}$. Having referred to relationships (56) and (57), taking the derivative of $\mathbf{s}'_{n+1}$ with respect to $\mathbf{e}_{n+1}$ means figuring $\partial \mathbf{X}^{\mathrm{S}}_{n+1}/\partial \mathbf{e}_{n+1}$ and $\partial X^{\mathrm{R}}_{n+1}/\partial \mathbf{e}_{n+1}$. Expanding Eq. (43), $\mathbf{X}^{\mathrm{S}}_{n+1}$ and X^{R}_{n+1} are determined, as follows:

$$\mathbf{X}^{\mathrm{S}}_{n+1} = \mathbf{X}^{\mathrm{S}}_{n+\alpha} + (a_{n+\alpha} - 1)(\Delta\hat{\boldsymbol{\mu}}^{\mathrm{T}}\mathbf{X}^{\mathrm{S}}_{n+\alpha})\Delta\hat{\boldsymbol{\mu}} + b_{n+\alpha}X^{\mathrm{R}}_{n+\alpha}\Delta\hat{\boldsymbol{\mu}} \tag{112}$$

$$X^{\mathrm{R}}_{n+1} = b_{n+\alpha}\Delta\hat{\boldsymbol{\mu}}^{\mathrm{T}}\mathbf{X}^{\mathrm{S}}_{n+\alpha} + a_{n+\alpha}X^{\mathrm{R}}_{n+\alpha} \tag{113}$$

In these formulas, the subscript $n+\alpha$ denotes the variables on the yield surface. Using Equalities (44) and (51)–(53) lead to the below values for $\mathbf{X}^{\mathrm{S}}_{n+\alpha}$ and $X^{\mathrm{R}}_{n+\alpha}$

$$\mathbf{X}^{\mathrm{S}}_{n+\alpha} = \mathbf{X}^{\mathrm{S}}_{n} + 2G\alpha X^{0}_{n}\Delta\mathbf{e} \tag{114}$$

Downloaded From: http://materialstechnology.asmedigitalcollection.asme.org/ on 05/25/2013 Terms of Use: http://asme.org/terms

$$X^{\mathrm{R}}_{n+\alpha} = X^{\mathrm{R}}_{n} - \sqrt{2}\alpha\beta \mathrm{K} X^{0}_{n}\Delta\varepsilon_{\mathrm{v}} \tag{115}$$

By exploiting the pervious equalities, the following derivatives can be found:

$$\begin{aligned}\frac{\partial \mathbf{X}^{\mathrm{S}}_{n+1}}{\partial \mathbf{e}_{n+1}} &= \frac{\partial \mathbf{X}^{\mathrm{S}}_{n+\alpha}}{\partial \mathbf{e}_{n+1}} + (\Delta\hat{\boldsymbol{\mu}}^{\mathrm{T}}\mathbf{X}^{\mathrm{S}}_{n+\alpha})\Delta\hat{\boldsymbol{\mu}}\left(\frac{\partial a_{n+\alpha}}{\partial \mathbf{e}_{n+1}}\right)^{\mathrm{T}} \\ &\quad + \Delta\hat{\boldsymbol{\mu}}\big((a_{n+\alpha}-1)\mathbf{Q}_1^{\mathrm{T}} + \mathbf{Q}_2^{\mathrm{T}}\big) + \big((a_{n+\alpha}-1)(\Delta\hat{\boldsymbol{\mu}}^{\mathrm{T}}\mathbf{X}^{\mathrm{S}}_{n+\alpha}) \\ &\quad + b_{n+\alpha}X^{\mathrm{R}}_{n+\alpha}\big)\frac{\partial \Delta\hat{\boldsymbol{\mu}}}{\partial \mathbf{e}_{n+1}}\end{aligned} \tag{116}$$

The vectors $\mathbf{Q}_1$ and $\mathbf{Q}_2$ are defined as below

$$\mathbf{Q}_1 = \left(\frac{\partial \Delta\hat{\boldsymbol{\mu}}}{\partial \mathbf{e}_{n+1}}\mathbf{X}^{\mathrm{S}}_{n+\alpha} + \frac{\partial \mathbf{X}^{\mathrm{S}}_{n+\alpha}}{\partial \mathbf{e}_{n+1}}\Delta\hat{\boldsymbol{\mu}}\right) \tag{117}$$

$$\mathbf{Q}_2 = \left(\frac{\partial b_{n+\alpha}}{\partial \mathbf{e}_{n+1}}X^{\mathrm{R}}_{n+\alpha} + b_{n+\alpha}\frac{\partial X^{\mathrm{R}}_{n+\alpha}}{\partial \mathbf{e}_{n+1}}\right) \tag{118}$$

$$\frac{\partial X^{\mathrm{R}}_{n+1}}{\partial \mathbf{e}_{n+1}} = \frac{\partial a_{n+\alpha}}{\partial \mathbf{e}_{n+1}}X^{\mathrm{R}}_{n+\alpha} + a_{n+\alpha}\frac{\partial X^{\mathrm{R}}_{n+\alpha}}{\partial \mathbf{e}_{n+1}} + b_{n+\alpha}\mathbf{Q}_1 + \frac{\partial b_{n+\alpha}}{\partial \mathbf{e}_{n+1}}(\Delta\hat{\boldsymbol{\mu}}^{\mathrm{T}}\mathbf{X}^{\mathrm{S}}_{n+\alpha}) \tag{119}$$

The following relations will be resulted if Eqs. (114) and (115) are used:

$$\frac{\partial \mathbf{X}^{\mathrm{S}}_{n+\alpha}}{\partial \mathbf{e}_{n+1}} = 2G\frac{\partial \alpha}{\partial \mathbf{e}_{n+1}}X^{0}_{n}\Delta\mathbf{e}^{\mathrm{T}} + 2G\alpha X^{0}_{n}\mathbb{I} \tag{120}$$

$$\frac{\partial X^{\mathrm{R}}_{n+\alpha}}{\partial \mathbf{e}_{n+1}} = -\sqrt{2}\beta K X^{0}_{n}\frac{\partial \alpha}{\partial \mathbf{e}_{n+1}}\Delta\varepsilon_{\mathrm{v}} \tag{121}$$

The $\partial\alpha/\partial\mathbf{e}_{n+1}$ is presented in the Appendix D. Appendix E gives the derivatives of $a_{n+\alpha}$, $b_{n+\alpha}$, and $\Delta\hat{\boldsymbol{\mu}}$ with respect to $\mathbf{e}_{n+1}$ introduced in relations (116) to (119).

Now that $\partial\mathbf{X}^{\mathrm{S}}_{n+1}/\partial\mathbf{e}_{n+1}$ and $\partial X^{\mathrm{R}}_{n+1}/\partial\mathbf{e}_{n+1}$ are known, one can manage to obtain $\partial\mathbf{s}'_{n+1}/\partial\mathbf{e}_{n+1}$ using Eqs. (56) and (57)

$$\frac{\partial \mathbf{s}'_{n+1}}{\partial \mathbf{e}_{n+1}} = \frac{R_{n+1}}{X^{\mathrm{R}}_{n+1}}\frac{\partial \mathbf{X}^{\mathrm{S}}_{n+1}}{\partial \mathbf{e}_{n+1}} - \frac{R_{n+1}}{(X^{\mathrm{R}}_{n+1})^2}\mathbf{X}^{\mathrm{S}}_{n+1}\left(\frac{\partial X^{\mathrm{R}}_{n+1}}{\partial \mathbf{e}_{n+1}}\right)^{\mathrm{T}} \tag{122}$$

To derive the derivative of the back stress vector with respect to the deviatoric strain, $\partial\boldsymbol{\alpha}_{n+1}/\partial\mathbf{e}_{n+1}$, Eq. (60) is hired, which results in the coming relationship

$$\frac{\partial \boldsymbol{\alpha}_{n+1}}{\partial \mathbf{e}_{n+1}} = \sum_{i=1}^{m} H_{\mathrm{kin},i}\frac{\partial \Delta\mathbf{e}^{\mathrm{p}}}{\partial \mathbf{e}_{n+1}} - \sum_{i=1}^{m} H_{\mathrm{nl},i}\boldsymbol{\alpha}_{n,i}\left(\frac{\partial \lambda}{\partial \mathbf{e}_{n+1}}\right)^{\mathrm{T}} \tag{123}$$

In this equality, $\partial\lambda/\partial\mathbf{e}_{n+1}$ is calculated akin to the one described in Appendix D for the forward Euler. To obtain $\partial\Delta\mathbf{e}^{\mathrm{p}}/\mathbf{e}_{n+1}$, one can use either Eqs. (63) or (64) corresponding the two approaches explained in Sec. 3.1. Following the first approach and Using Eq. (63) alongside Eq. (56), the next formula can be derived

$$\begin{aligned}\frac{\partial \Delta\mathbf{e}^{\mathrm{p}}}{\partial \mathbf{e}_{n+1}} &= \left[\frac{\mathbf{s}'_n}{2\bar{G}X^{0}_{n+1}R_{n+1}} + \frac{G\alpha\Delta\mathbf{e}}{\bar{G}X^{0}_{n+1}R_{n+1}}\right]\left(\frac{\partial X^{\mathrm{R}}_{n+1}}{\partial \mathbf{e}_{n+1}}\right)^{\mathrm{T}} \\ &\quad + \frac{G\ln(X^{0}_{n+1})}{\bar{G}}\left(\Delta\mathbf{e}\left(\frac{\partial \alpha}{\partial \mathbf{e}_{n+1}}\right)^{\mathrm{T}} + \alpha\mathbb{I}\right)\end{aligned} \tag{124}$$

where $\partial X^{\mathrm{R}}_{n+\alpha}/\partial\mathbf{e}_{n+1}$ is known by Eq. (121) and $\partial\alpha/\partial\mathbf{e}_{n+1}$ is presented in Appendix D. On the other hand, having pursued the second approach and used Eq. (64), $\partial\Delta\mathbf{e}^{\mathrm{p}}/\partial\mathbf{e}_{n+1}$ is computed in the following form:

$$\frac{\partial \Delta\mathbf{e}^{\mathrm{p}}}{\partial \mathbf{e}_{n+1}} = \frac{1}{2\bar{G}}\left(2G\mathbb{I} - \frac{\partial \bar{\mathbf{a}}}{\partial \mathbf{e}_{n+1}} - \frac{\partial \mathbf{s}'_{n+1}}{\partial \mathbf{e}_{n+1}}\right) \tag{125}$$

The term of $\partial\mathbf{s}'_{n+1}/\partial\mathbf{e}_{n+1}$ has already been acquired through relationship (122) and $\partial\bar{\mathbf{a}}/\partial\mathbf{e}_{n+1}$ is given by the next equality, which has been derived via Eq. (65)

$$\frac{\partial \bar{\mathbf{a}}}{\partial \mathbf{e}_{n+1}} = \sum_{i=1}^{m}\frac{-H_{\mathrm{nl},i}}{2\bar{G}R_{n+1}X^{0}_{n+1}}\boldsymbol{\alpha}_{n,i}\left(\frac{\partial X^{\mathrm{R}}_{n+1}}{\partial \mathbf{e}_{n+1}}\right)^{\mathrm{T}} \tag{126}$$

5.4 Semi-Implicit Exponential Consistent Tangent Modulus. To reach the tangent modulus consistent with the scheme, it is needed to calculate the derivatives of the deviatoric shifted stress and the back stress at the specified point of each load increment, which is designated by $\xi, 0 < \xi < 1$. This means computing $\partial\mathbf{s}'_{n+\xi(1-\alpha)}/\partial\mathbf{e}_{n+1}$ and $\partial\boldsymbol{\alpha}_{n+\xi(1-\alpha)}/\partial\mathbf{e}_{n+1}$. By referring to relationships (74), $\partial\mathbf{s}'_{n+\xi(1-\alpha)}/\partial\mathbf{e}_{n+1}$ is attained, as follows:

$$\begin{aligned}\frac{\partial \mathbf{s}'_{n+\xi(1-\alpha)}}{\partial \mathbf{e}_{n+1}} &= \frac{R_{n+\xi(1-\alpha)}}{X^{\mathrm{R}}_{n+\xi(1-\alpha)}}\frac{\partial \mathbf{X}^{\mathrm{S}}_{n+\xi(1-\alpha)}}{\partial \mathbf{e}_{n+1}} \\ &\quad - \frac{R_{n+\xi(1-\alpha)}}{(X^{\mathrm{R}}_{n+\xi(1-\alpha)})^2}\mathbf{X}^{\mathrm{S}}_{n+\xi(1-\alpha)}\left(\frac{\partial X^{\mathrm{R}}_{n+\xi(1-\alpha)}}{\partial \mathbf{e}_{n+\xi(1-\alpha)}}\right)^{\mathrm{T}}\end{aligned} \tag{127}$$

where using Eqs. (66) and (67), $\partial\mathbf{X}^{\mathrm{S}}_{n+\xi(1-\alpha)}/\partial\mathbf{e}_{n+1}$ and $\partial X^{\mathrm{R}}_{n+\xi(1-\alpha)}/\partial\mathbf{e}_{n+1}$ are obtained through the subsequent relationships

$$\begin{aligned}\frac{\partial \mathbf{X}^{\mathrm{S}}_{n+\xi(1-\alpha)}}{\partial \mathbf{e}_{n+1}} &= \frac{\partial \mathbf{X}^{\mathrm{S}}_{n+\alpha}}{\partial \mathbf{e}_{n+1}} + (\Delta\hat{\boldsymbol{\mu}}^{\xi\mathrm{T}}_{n+\alpha}\mathbf{X}^{\mathrm{S}}_{n+\alpha})\Delta\hat{\boldsymbol{\mu}}^{\xi}_{n+\alpha}\left(\frac{\partial a^{\xi}_{n+\alpha}}{\partial \mathbf{e}_{n+1}}\right)^{\mathrm{T}} \\ &\quad + \Delta\hat{\boldsymbol{\mu}}^{\xi}_{n+\alpha}\Big((a^{\xi}_{n+\alpha}-1)\mathbf{Q}^{\xi}_1 + \mathbf{Q}^{\xi}_2\Big)^{\mathrm{T}} \\ &\quad + \big((a^{\xi}_{n+\alpha}-1)(\Delta\hat{\boldsymbol{\mu}}^{\xi}_{n+\alpha}{}^{\mathrm{T}}\mathbf{X}^{\mathrm{S}}_{n+\alpha}) + b^{\xi}_{n+\alpha}X^{\mathrm{R}}_{n+\alpha}\big) \\ &\quad \times \frac{\partial \Delta\hat{\boldsymbol{\mu}}^{\xi}_{n+\alpha}}{\partial \mathbf{e}_{n+1}}\end{aligned} \tag{128}$$

In this equation, $\mathbf{Q}^{\xi}_1$ and $\mathbf{Q}^{\xi}_2$ are defined by the below formulas

$$\mathbf{Q}^{\xi}_1 = \left(\frac{\partial \Delta\hat{\boldsymbol{\mu}}^{\xi}_{n+\alpha}}{\partial \mathbf{e}_{n+1}}\mathbf{X}^{\mathrm{S}}_{n+\alpha} + \frac{\partial \mathbf{X}^{\mathrm{S}}_{n+\alpha}}{\partial \mathbf{e}_{n+1}}\Delta\hat{\boldsymbol{\mu}}^{\xi}_{n+\alpha}\right) \tag{129}$$

$$\mathbf{Q}^{\xi}_2 = \left(\frac{\partial b^{\xi}_{n+\alpha}}{\partial \mathbf{e}_{n+1}}X^{\mathrm{R}}_{n+\alpha} + b^{\xi}_{n+\alpha}\frac{\partial X^{\mathrm{R}}_{n+\alpha}}{\partial \mathbf{e}_{n+1}}\right) \tag{130}$$

$$\begin{aligned}\frac{\partial X^{\mathrm{R}}_{n+\xi(1-\alpha)}}{\partial \mathbf{e}_{n+1}} &= \frac{\partial a^{\xi}_{n+\alpha}}{\partial \mathbf{e}_{n+1}}X^{\mathrm{R}}_{n+\alpha} + a^{\xi}_{n+\alpha}\frac{\partial X^{\mathrm{R}}_{n+\alpha}}{\partial \mathbf{e}_{n+1}} + b^{\xi}_{n+\alpha}\mathbf{Q}^{\xi}_1 \\ &\quad + \frac{\partial b^{\xi}_{n+\alpha}}{\partial \mathbf{e}_{n+1}}(\Delta\hat{\boldsymbol{\mu}}^{\xi}_{n+\alpha}\mathrm{T}\mathbf{X}^{\mathrm{S}}_{n+\alpha})\end{aligned} \tag{131}$$

To avoid any confusion and since the procedure of achieving the tangent modulus is in the first degree of importance to the authors than the derivatives themselves, the details of the calculations related to the former equations are given in Appendix F. The term of $\partial\boldsymbol{\alpha}_{n+\xi(1-\alpha)}/\partial\mathbf{e}_{n+1}$ is derived from Eq. (75), as follows:

$$\frac{\partial \boldsymbol{\alpha}_{n+\xi(1-\alpha)}}{\partial \mathbf{e}_{n+1}} = \sum_{i=1}^{m}\frac{\partial \bar{\mathbf{a}}_{n,i}}{\partial \mathbf{e}_{n+1}} + \sum_{i=1}^{m}\frac{\partial \bar{H}_i}{\partial \mathbf{e}_{n+1}}\Delta\mathbf{e}^{\mathrm{p}}_{n+\xi(1-\alpha)} + \sum_{i=1}^{m}\bar{H}_i\frac{\partial \Delta\mathbf{e}^{\mathrm{p}}_{n+\xi(1-\alpha)}}{\partial \mathbf{e}_{n+1}} \tag{132}$$

The values of $\partial\bar{\mathbf{a}}_{n,i}/\partial\mathbf{e}_{n+1}$, $\partial\bar{H}_i/\partial\mathbf{e}_{n+1}$, and $\partial\Delta\mathbf{e}^{\mathrm{p}}_{n+\xi(1-\alpha)}/\partial\mathbf{e}_{n+1}$ will be presented in Appendix F.

Now that, the derivatives of $\boldsymbol{\alpha}$ and $\mathbf{s}'$ are known at the specified point denoted by ξ, $\partial\boldsymbol{\sigma}_{n+1}/\partial\mathbf{e}_{n+1}$ will be acquired by performing

Downloaded From: http://materialstechnology.asmedigitalcollection.asme.org/ on 05/25/2013 Terms of Use: http://asme.org/terms

the whole process again, but this time using $\partial \mathbf{s}'_{n+\xi(1-\alpha)}/\partial \mathbf{e}_{n+1}$ and $\partial \boldsymbol{\alpha}_{n+\xi(1-\alpha)}/\partial \mathbf{e}_{n+1}$ instead of $\partial \mathbf{s}'_{n+\alpha}/\partial \mathbf{e}_{n+1}$ and $\partial \boldsymbol{\alpha}_{n+\alpha}/\partial \mathbf{e}_{n+1}$, respectively. It means that the following relationship, which has been obtained from Eqs. (56) and (57), computes $\partial \mathbf{s}'_{n+1}/\partial \mathbf{e}_{n+1}$:

$$\frac{\partial \mathbf{s}'_{n+1}}{\partial \mathbf{e}_{n+1}} = \frac{R_{n+1}}{X^{\mathrm{R}}_{n+1}}\frac{\partial \mathbf{X}^{\mathrm{S}}_{n+1}}{\partial \mathbf{e}_{n+1}} - \frac{R_{n+1}}{\left(X^{\mathrm{R}}_{n+1}\right)^2}\mathbf{X}^{\mathrm{S}}_{n+1}\left(\frac{\partial X^{\mathrm{R}}_{n+1}}{\partial \mathbf{e}_{n+1}}\right)^{\mathrm{T}} \tag{133}$$

To avoid lengthening, $\partial \mathbf{X}^{\mathrm{S}}_{n+1}/\partial \mathbf{e}_{n+1}$ and $\partial X^{\mathrm{R}}_{n+1}/\partial \mathbf{e}_{n+1}$ are introduced in Appendix F. Equation (87) is utilized to reach the below relationship for $\partial \alpha_{n+1}/\partial \mathbf{e}_{n+1}$

$$\frac{\partial \boldsymbol{\alpha}_{n+1}}{\partial \mathbf{e}_{n+1}} = \sum_{i=1}^{m} H_{\mathrm{kin},i}\frac{\partial \Delta \mathbf{e}^{\mathrm{p}}}{\partial \mathbf{e}_{n+1}} - \sum_{i=1}^{m} H_{\mathrm{nl},i}\boldsymbol{\alpha}_{n+\xi(1-\alpha),i}\left(\frac{\partial \lambda_{n+\xi(1-\alpha)}}{\partial \mathbf{e}_{n+1}}\right)^{\mathrm{T}} \tag{134}$$

Appendix F presents $\partial \lambda_{n+\xi(1-\alpha)}/\partial \mathbf{e}_{n+1}$ in this equality. $\partial \Delta \mathbf{e}^{\mathrm{p}}/\mathbf{e}_{n+1}$ is calculated via Eq. (125), in which, $\partial \bar{\mathbf{a}}/\partial \mathbf{e}_{n+1}$ is derived using Equality (88), as follows:

$$\frac{\partial \bar{\mathbf{a}}}{\partial \mathbf{e}_{n+1}} = \sum_{i=1}^{m} \frac{-H_{\mathrm{nl},i}}{2\bar{G}R_{n+1}X^{0}_{n+1}}\boldsymbol{\alpha}_{n+\xi(1-\alpha),i}\left(\frac{\partial X^{\mathrm{R}}_{n+1}}{\partial \mathbf{e}_{n+1}}\right)^{\mathrm{T}} - \frac{H_{\mathrm{nl},i}}{2\bar{G}}\ln(X^{0}_{n+1})\frac{\partial \boldsymbol{\alpha}_{n+\xi(1-\alpha)}}{\partial \mathbf{e}_{n+1}} \tag{135}$$

where $\partial X^{\mathrm{R}}_{n+\xi(1-\alpha)}/\partial \mathbf{e}_{n+1}$ and $\partial \boldsymbol{\alpha}_{n+\xi(1-\alpha)}/\partial \mathbf{e}_{n+1}$ have already been attained through Eqs. (131) and (132), respectively. $\partial R_{n+\xi(1-\alpha)}/\partial \mathbf{e}_{n+1}$ will be presented in Appendix F and other parameters are also known by means of prior relationships.

6 Verifying the Suggested Formulations

A body of point-wise numerical examples is presented in this section to validate the proposed algorithms. Three general types of numerical tests are taken to investigate the accuracy and performance of the formulations, including stress and strain-updating tests along with a boundary value problem. At the first category, for a given strain history, stresses will be updated using the classical integrations of Forward and backward Euler and the newly developed exponential-based techniques consisting of fully explicit and semi-implicit. Having updated the stresses via the four integrating methods, the results are compared in three major grounds of accuracy, convergence rate, and performance using illustrative graphs and lucid tables.

The second category of numerical experiences is adopted to ascertain the tangent operators of the classical and suggested schemes. In this group of examples, the derived tangent operators of the proposed schemes are examined using the strain-updating examples, which means computing strain histories for a variety of stress paths. The examination includes accuracy investigation and verification of the asymptotic quadratic convergence rate of the developed consistent tangent moduli.

In order for these tests to have a comprehensive comparison, two different histories of strains and two different histories of stresses are adopted for the stress and strain-updating tests, respectively. To avoid the discretization errors, all the strain and stress histories are considered linear. It is also necessary to mention that, due to the absence of the analytical solutions of the investigated problems, the results of the numerical techniques are compared with those of backward Euler method with a very small load-step size (100,000 steps per second), which is considered as the exact solution.

Eventually, a boundary value problem is chosen to be solved using each algorithm in a nonlinear finite-element code to verify the proposed strategies and the tangent operators in rendering the asymptotic quadratic convergence rate in actuality. The problem is comprised of a rectangular strip having an elliptical hole in its center under a uniform load.

As it was mentioned earlier, this study is to introduce two new exponential-based integrations for the pressure-sensitive nonassociative plasticity model proposed by Lei and Lissenden [14] for DRA composites. Therefore, the mechanical properties of the DRA system 6092/SiC/17.5p-T6 are taken into account drawn from Ref. [14]. The linear elastic parameters of the material are given below

$$E = 102,000\ \mathrm{MPa} \quad \nu = 0.325 \quad G = 38,500\ \mathrm{MPa}$$

The yield-surface parameters include the following values:

$$\tau_{y,0} = 220/\sqrt{2}\ \mathrm{MPa} \quad \beta = 0.078/\sqrt{2}$$

This DRA system consists of the subsequent material hardening parameters

$$H_{\mathrm{kin},1} = 220,000\ \mathrm{MPa} \quad H_{\mathrm{nl},1} = 3200$$
$$H_{\mathrm{kin},2} = 24,000\ \mathrm{MPa} \quad H_{\mathrm{nl},2} = 400$$
$$H_{\mathrm{kin},3} = 3200\ \mathrm{MPa} \quad H_{\mathrm{nl},3} = 35$$

For the sake of brevity and conciseness, abbreviations below are used to represent the methods:

FE: Forward Euler integrating method and its tangent modulus
BE: Backward Euler integrating method and its tangent modulus
EXF: Fully explicit exponential map integrating method and its tangent modulus
EXS: Semi-implicit exponential map integrating method and its tangent modulus

6.1 Stress-Updating Tests. This section is subject to a broad set of numerical tests, where the new algorithms are examined in three different areas, including the accuracy, performance, and accuracy convergence rate. Figures 4 and 5 illustrate the two biaxial nonproportional strain histories considered for the purpose. Each strain history is regulated by two strain components varied proportionally to the first yielding strain, $\varepsilon_{y,0}$, in a uniaxial loading history. Other strain components are considered equal to zero.

Test 1: ε_{11} and ε_{12}
Test 2: ε_{11} and ε_{22}

$$\varepsilon_{y,0} = \frac{\sqrt{3}\tau_{y,0}}{2G} \tag{136}$$

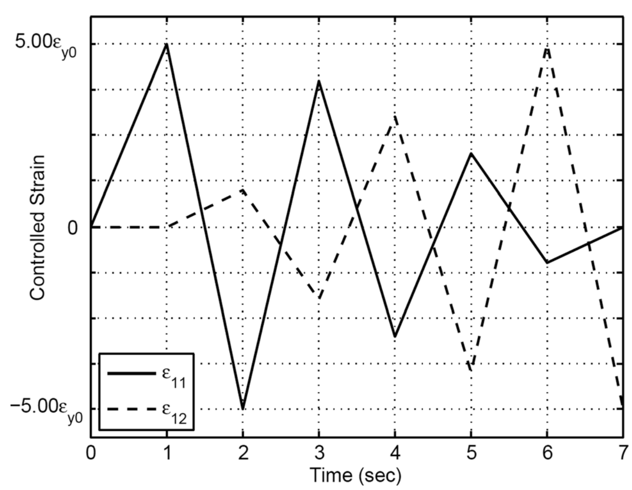

Fig. 4 Strain history 1

Downloaded From: http://materialstechnology.asmedigitalcollection.asme.org/ on 05/25/2013 Terms of Use: http://asme.org/terms

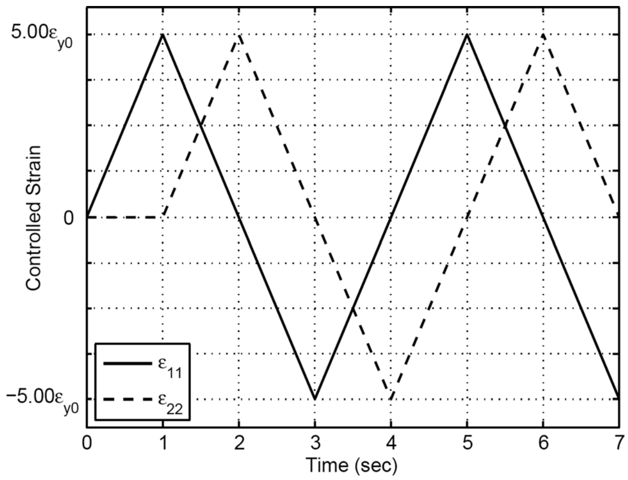

Fig. 5 Strain history 2

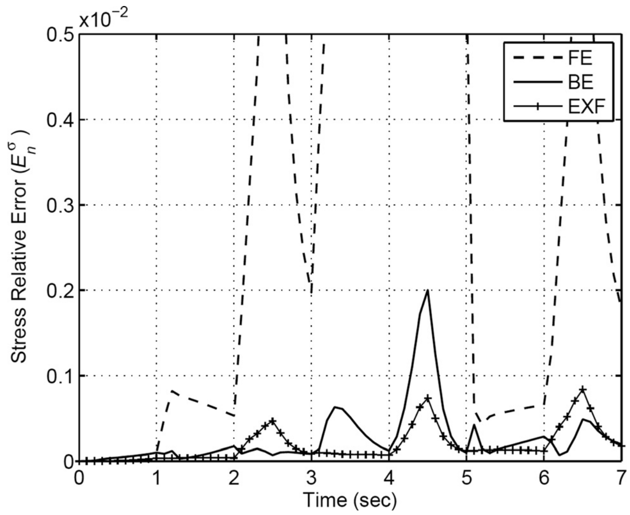

Fig. 8 Stress relative errors by FE, BE, and EXF for strain history 2

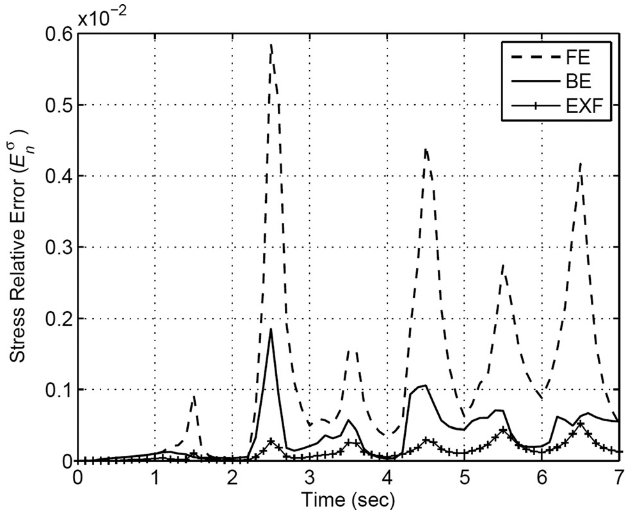

Fig. 6 Stress relative errors by FE, BE, and EXF for strain history 1

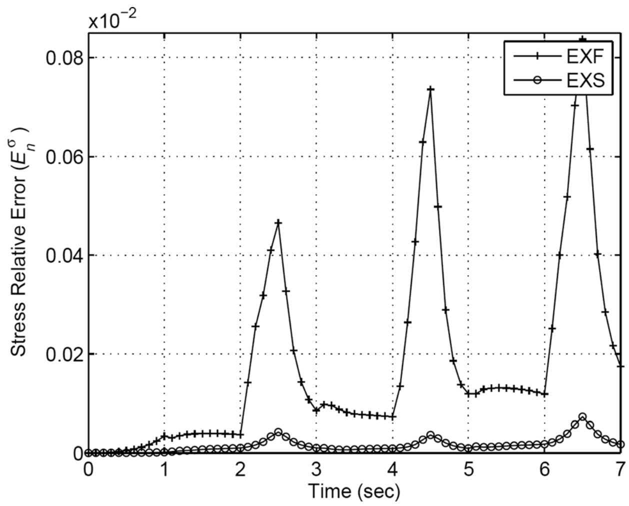

Fig. 9 Stress relative errors by EXF and EXS for strain history 2

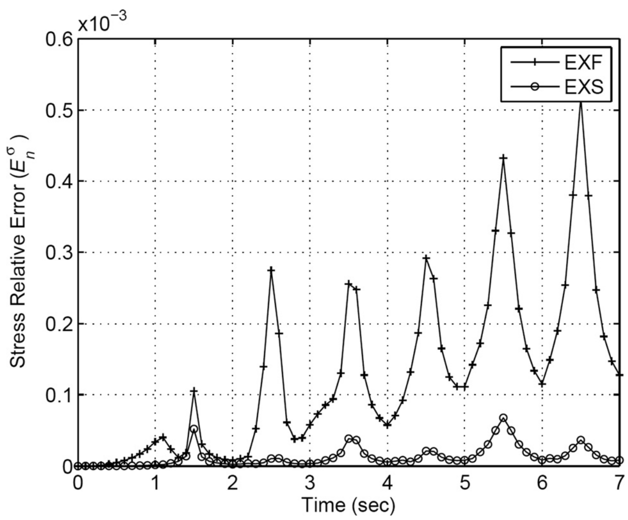

Fig. 7 Stress relative errors by EXF and EXS for strain history 1

To investigate the accuracy of the new formulations, stress relative error of the Euler's and the suggested methods are calculated and compared with each other. The error is obtained through the following relationship, where $\bar{\boldsymbol{\sigma}}_n$ and $\boldsymbol{\sigma}_n$ are, respectively, the numerical and the exact updated stresses at time t_n

$$E_n^{\boldsymbol{\sigma}} = \frac{\|\boldsymbol{\sigma}_n - \bar{\boldsymbol{\sigma}}_n\|}{\|\boldsymbol{\sigma}_n\|} \tag{137}$$

Figures 6–9 display the plotted errors of the Euler's, FE and BE, and the suggested schemes, EXF and EXS, against the time for the practical time step size of $\Delta t = 0.025$. Since EXS is much more accurate that cannot be perceived in one diagram with others, it is compared to EXF in different graphs for each strain history.

As it is obvious in all diagrams, the accuracy of the updated stresses from FE is less than the other three methods by a long way. The precision of BE and EXF are either approximately the same or EXF is better than BE but not much. Remarkably, EXS has a greater accuracy compared to the others. The preciseness of EXS is in a huge extent that even for a large step size like $\Delta t = 0.1$s, it has already achieved such good results that are comparable with those of BE or EXF with small step sizes of

Downloaded From: http://materialstechnology.asmedigitalcollection.asme.org/ on 05/25/2013 Terms of Use: http://asme.org/terms

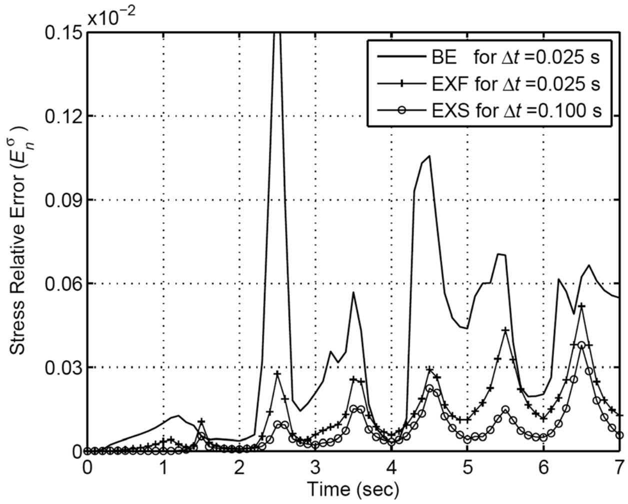

Fig. 10 Comparison of the accuracy of EXF and BE with EXS for strain history 1

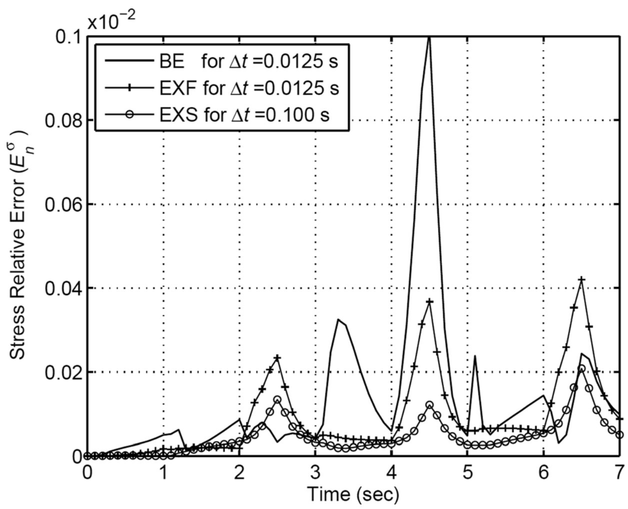

Fig. 11 Comparison of the accuracy of EXF and BE with EXS for strain history 2

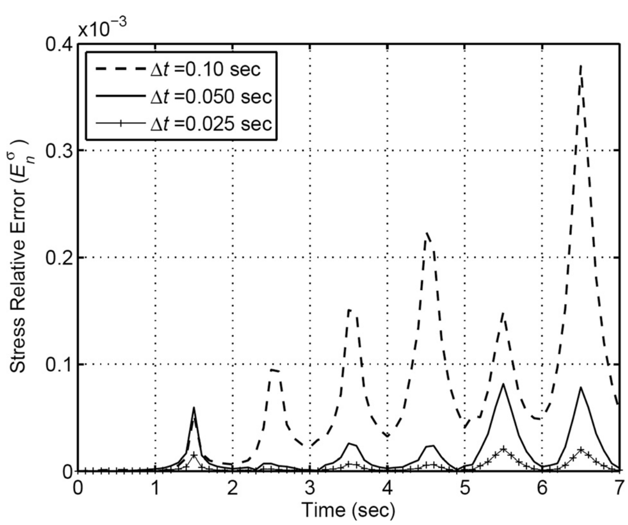

Fig. 12 Stress relative error by EXS in consecutive load-step sizes for strain history 1

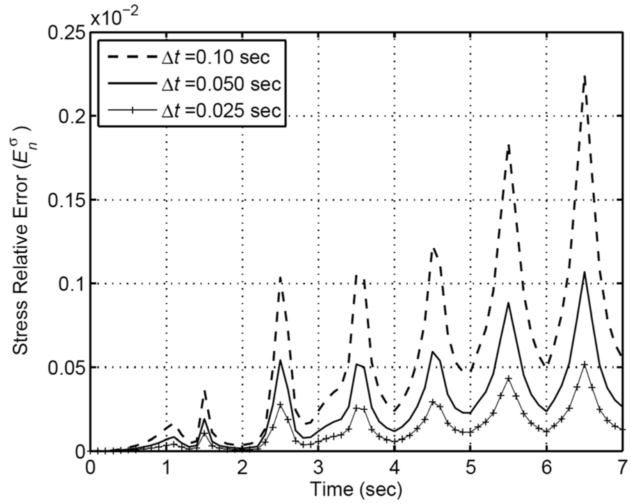

Fig. 13 Stress relative error by EXF in consecutive load-step sizes for strain history 1

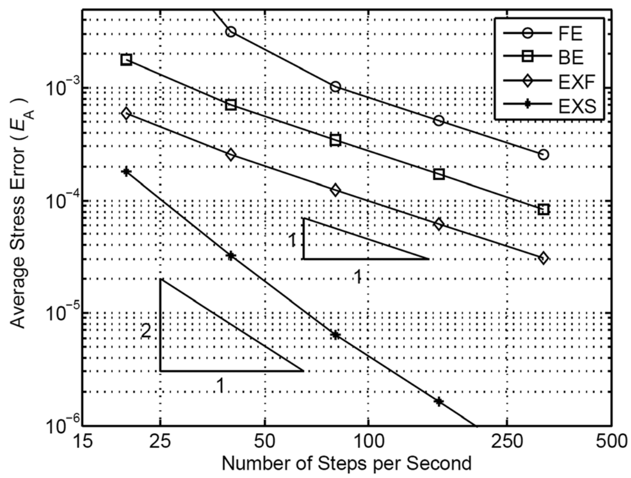

Fig. 14 Demonstration of the accuracy convergence rates of the integration schemes for strain history 1

$\Delta t = 0.025$ and 0.0125 s. See, for example, Figs. 10 and 11. The reason is the convergence rate.

The convergence rates of the recommended strategies, EXF and EXS, are verified by computing their relative errors for different load-step sizes, as it is shown in Figs. 12 and 13. The diagrams prove that the EXS rapidly converges on the exact solution. Having computed the average stress errors of the new and classical tactics and plotted them against each other, their convergence rates are thoroughly investigated, as it is shown in Fig. 14. While linear convergence rate is discerned for EXF, like BE and FE, the convergence rate of EXS is quadratic. That is why its convergence begins from large step sizes such as $\Delta t = 0.3$ s and by $\Delta t = 0.025$ s it has a nearly exact response with the accuracy of 10^{-5}. At this point, a significant question is, how long does it take for EXF or EXS to get to the response? Are they fast enough to defeat the classical methods of FE and BE? These questions are replied by computational efficiency or performance.

Performance is the most important fact of the numerical approaches, which means putting accuracy in front of the computational time. To investigate performance of the integrating schemes, the following relationship is adopted:

$$\eta = \frac{\text{Accuracy}}{\text{Computational time}} = \frac{1}{E_{\text{A}} \times T_{\text{CPU}}} \tag{138}$$

Downloaded From: http://materialstechnology.asmedigitalcollection.asme.org/ on 05/25/2013 Terms of Use: http://asme.org/terms

Table 1 Performance of the integrating schemes for 200 cycles of the strain history 1

Integration scheme	Load-step size	E_T	E_A	$T_{CPU}(s)$	η
BE	0.2	25.2065	0.3600	8.52	0.33
	0.1	10.0374	0.1434	14.25	0.49
	0.05	4.8820	0.0697	23.76	0.60
	0.025	2.4112	0.0344	42.68	0.68
FE	0.2	581.1668	8.3012	1.13	0.11
	0.1	44.9087	0.6415	2.10	0.74
	0.05	14.4703	0.2067	4.04	1.20
	0.025	7.9068	0.1129	7.83	1.13
EXF	0.2	8.5027	0.1214	1.51	5.45
	0.1	3.6410	0.0520	2.73	7.04
	0.05	1.7678	0.0253	5.17	7.64
	0.025	0.8687	0.0124	10.16	7.94
EXS	0.2	2.5244	0.0361	2.41	11.49
	0.1	0.4566	0.0065	4.52	34.04
	0.05	0.0916	0.0013	8.57	89.76
	0.025	0.0248	0.0003	16.89	197.355

Table 2 Computational time of the schemes for 200 cycles of the strain histories 1 and 2

	Strain history 1		Strain history 2	
Integration scheme	Total error	CPU time (s)	Total error	CPU time (s)
FE	0.093	659.08	0.187	1204.20
BE	0.092	673.28	0.189	301.72
EXF	0.092	96.08	0.189	72.08
EXS	0.092	8.57	0.185	9.68

where, η, T_{CPU}, and E_A represent the performance, CPU time, and average error, respectively. Here, accuracy has been defined as the inverse of average error. To compare the performance of the suggested formulations with the classical integrating ones, average errors and CPU times are computed for 200 cycles of the strain history 1, whereby one can have more measurable CPU times and more accurate average errors. To have a better examination of the performance, this act is performed for a variety of load-step sizes. The results are presented in Table 1. Total error, E_T, which is the sum of the stress relative errors, divided by the number of points where the errors are calculated gives the average error. Moreover,

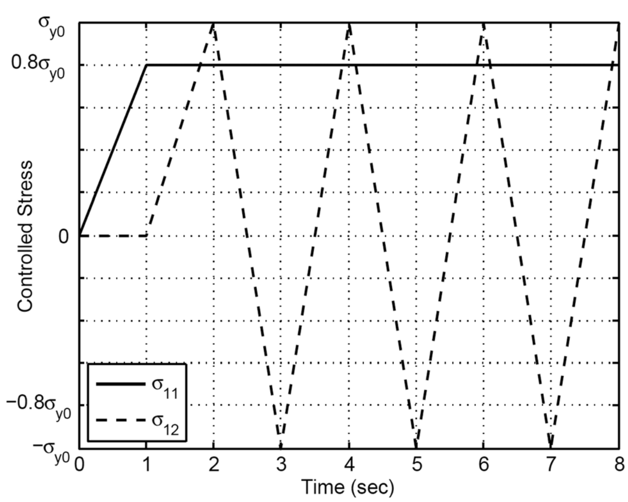

Fig. 15 Stress history 1

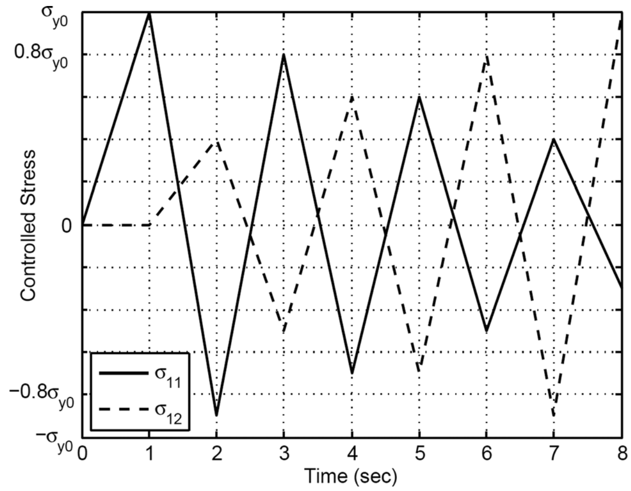

Fig. 16 Stress history 2

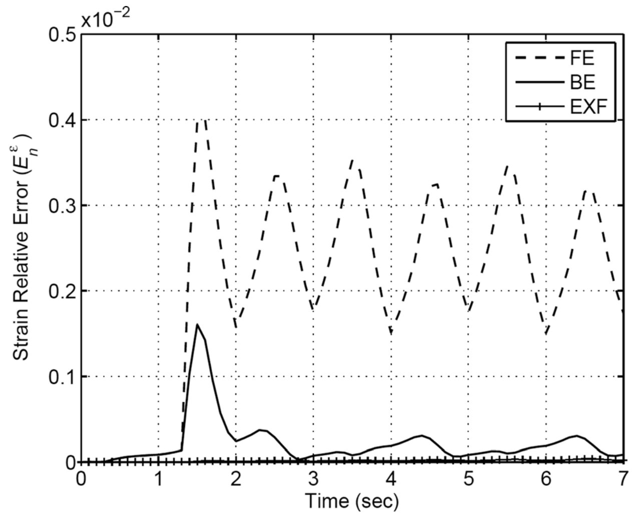

Fig. 17 Strain relative errors by FE, BE, and EXF for stress history 1

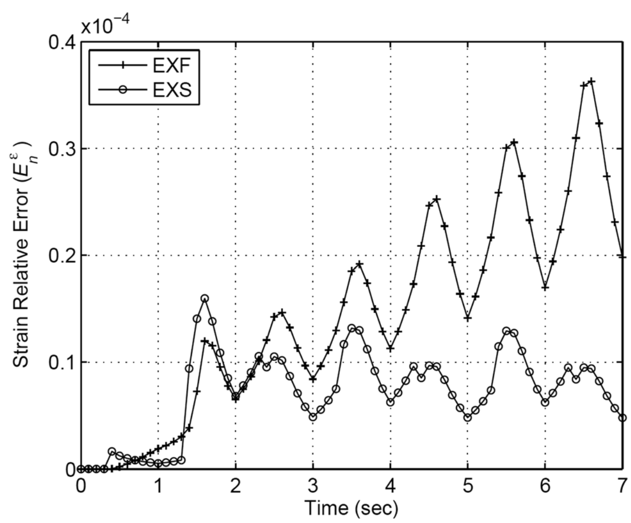

Fig. 18 Strain relative errors by EXF and EXS for stress history 1

Downloaded From: http://materialstechnology.asmedigitalcollection.asme.org/ on 05/25/2013 Terms of Use: http://asme.org/terms

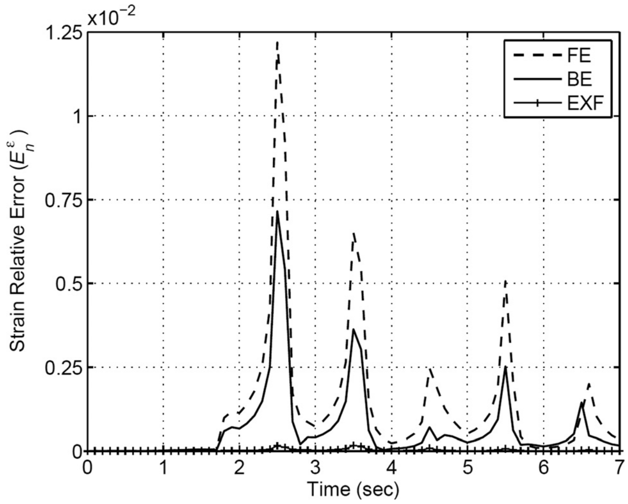

Fig. 19 Strain relative errors by FE, BE, and EXF for stress history 2

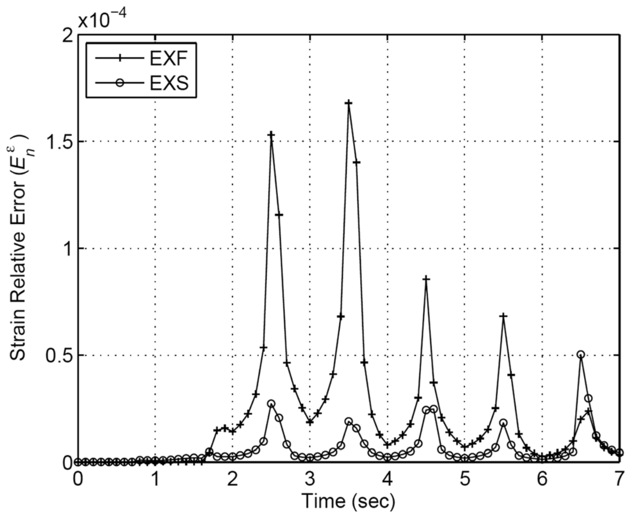

Fig. 20 Strain relative errors by EXF and EXS for stress history 2

Table 2 presents the computational efforts of the schemes in achieving the same accuracy as each other rendering another means of performance investigation. As it is evident in both tables, the performances of the new integrating schemes are much better than the Euler's schemes, particularly the EXS. Thanks to the very accurate responses alongside short CPU times, the EXS is the most efficient algorithm among the others. It is also deduced that by shortening the load-step size, the performance of FE, BE, and EXF tend to converge on a constant amount while the computational efficiency of the EXS will increase constantly. It is worth emphasizing that among the four presented integrating methodologies, unquestionably, the best integration for this nonassociative plasticity model is the EXS. The reason is its great preciseness and performance that it can be named virtually as an accurate integration than an approximate one.

6.2 Strain-Updating Tests. In this section, two different point-wise tests are considered to investigate the consistent tangent modulus of the suggested exponential map processes, EXF and EXS. In each test, for a given stress history, strain will be updated using the tangent operators of the suggested schemes and the ones of the forward Euler and backward Euler methods. The two stress histories are illustrated in Figs. 15 and 16. Using the strain-updating results of the forward Euler technique with a very fine load-step size of $\Delta t = 1 \times 10^{-5}$ as the exact solution, the accuracy of the EXF and EXS are assessed. The coming relationship obtains the relative strain error, E_n^ε

$$E_n^\varepsilon = \frac{\|\boldsymbol{\varepsilon}_n - \bar{\boldsymbol{\varepsilon}}_n\|}{\|\boldsymbol{\varepsilon}_n\|} \tag{139}$$

where $\boldsymbol{\varepsilon}_n$ represents the exact strain vector at time t_n and $\bar{\boldsymbol{\varepsilon}}_n$ stands for the numerical solution. Figures 17–20 display the relative strain errors of the methods in question compared to one another for both stress histories. Since the new exponential-based methods are much more accurate than the classical ones, EXF and EXS are graphed in separate diagrams similar to what were given for the stress relative errors. The results are presented for the practical load-step size of $\Delta t = 0.025$ s. Clearly, the EXF and EXS are much more accurate than FE and BE. The EXS also presents much better responses compared to the EXF. To examine the quadratic convergence rate of the tangent operators, it is needed to calculate the relative Euclidean norms of the errors for each time step, which are defined as below

Table 3 Relative Euclidian norms to demonstrate the tangent operators, stress path 1

	$t = 2$ s			$t = 6$ s		
Iteration	FE	EXF	EXS	FE	EXF	EXS
1	1.000×10	1.000×10	1.000×10	1.000×10	1.000×10	1.000×10
2	8.100×10^{-3}	2.300×10^{-3}	2.300×10^{-3}	9.700×10^{-3}	2.100×10^{-3}	2.100×10^{-3}
3	1.078×10^{-5}	6.332×10^{-6}	6.319×10^{-6}	1.120×10^{-5}	5.487×10^{-6}	5.505×10^{-6}
4	1.106×10^{-7}	1.457×10^{-8}	1.455×10^{-8}	1.330×10^{-7}	1.170×10^{-8}	1.179×10^{-8}
5	2.551×10^{-10}	4.069×10^{-11}	4.065×10^{-11}	1.461×10^{-11}	3.047×10^{-11}	3.077×10^{-11}

Table 4 Relative Euclidian norms to demonstrate the tangent operators, stress path 2

	$t = 2$ s			$t = 6$ s		
Iteration	FE	EXF	EXS	FE	EXF	EXS
1	1.000×10	1.000×10	1.000×10	1.000×10	1.000×10	1.000×10
2	2.900×10^{-3}	5.970×10^{-4}	6.063×10^{-4}	8.367×10^{-3}	1.826×10^{-4}	1.822×10^{-4}
3	1.825×10^{-5}	3.864×10^{-7}	3.851×10^{-7}	1.629×10^{-6}	3.637×10^{-8}	3.662×10^{-8}
4	5.178×10^{-9}	2.236×10^{-10}	2.254×10^{-10}	1.330×10^{-10}	6.362×10^{-12}	6.288×10^{-12}

Downloaded From: http://materialstechnology.asmedigitalcollection.asme.org/ on 05/25/2013 Terms of Use: http://asme.org/terms

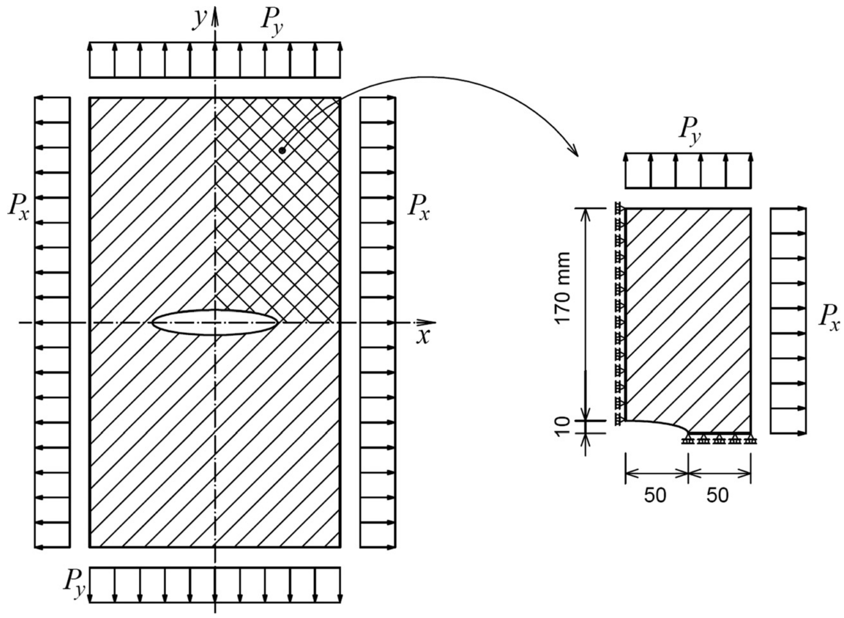

Fig. 21 The strip with an elliptical hole

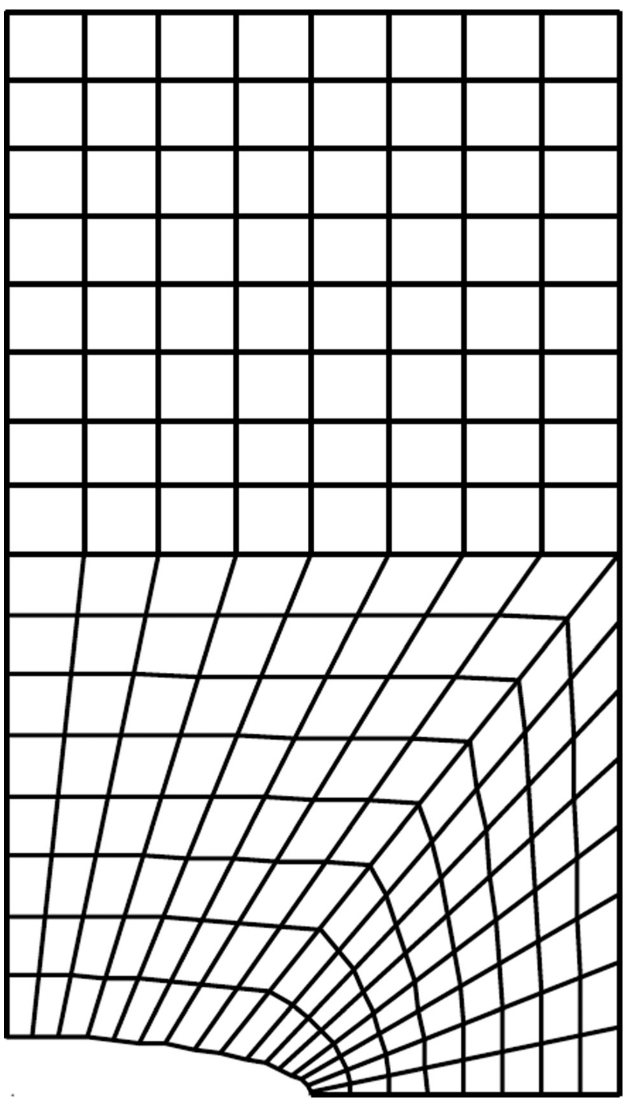

Fig. 22 The finite-element mesh

$$E_n^i = \frac{\left\| \boldsymbol{\varepsilon}_n^i - \boldsymbol{\varepsilon}_n \right\|}{\left\| \boldsymbol{\varepsilon}_n^1 - \boldsymbol{\varepsilon}_n \right\|} \tag{140}$$

In the former equality, $\boldsymbol{\varepsilon}_n$ is the converged strain and $\boldsymbol{\varepsilon}_n^i$ presents the converged strain at the ith iteration. To verify the quadratic convergence rate of the developed tangent operators, Tables 3 and 4 were prepared to illustrate the relative Euclidean errors of the tangent modulus of FE, EXF, and EXS in successive iterations for both stress histories in two arbitrary times, $t = 2$ s and $t = 6$ s.

At this stage, it is worth emphasizing that the quadratic convergence rate of the tangent operators has no connection with the convergence rate (accuracy order) of the integration schemes. Regardless of the convergence rate of an integration method, their tangent operators must always be capable of achieving the asymptotic quadratic convergence rate of the Newton–Raphson solution in nonlinear finite-element analyses.

6.3 Boundary Value Problem. In the following, a boundary value problem is solved by utilizing all the algorithms under discussion to feature the schemes' performance as well as proving the derived tangent operators in practice. Hence, using the path-

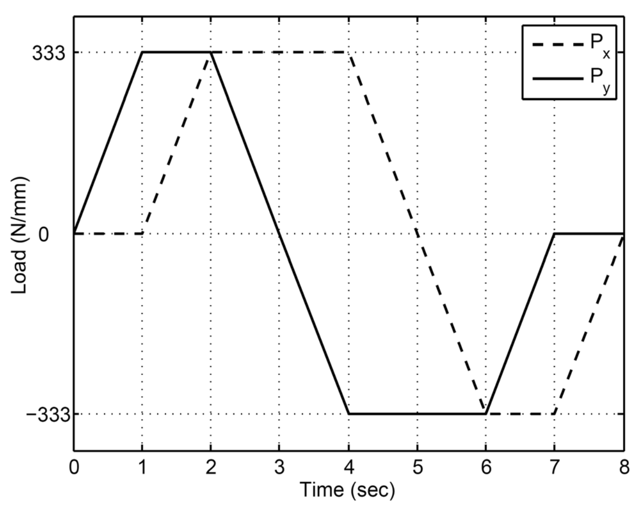

Fig. 23 The history of the nonproportional loads

Downloaded From: http://materialstechnology.asmedigitalcollection.asme.org/ on 05/25/2013 Terms of Use: http://asme.org/terms

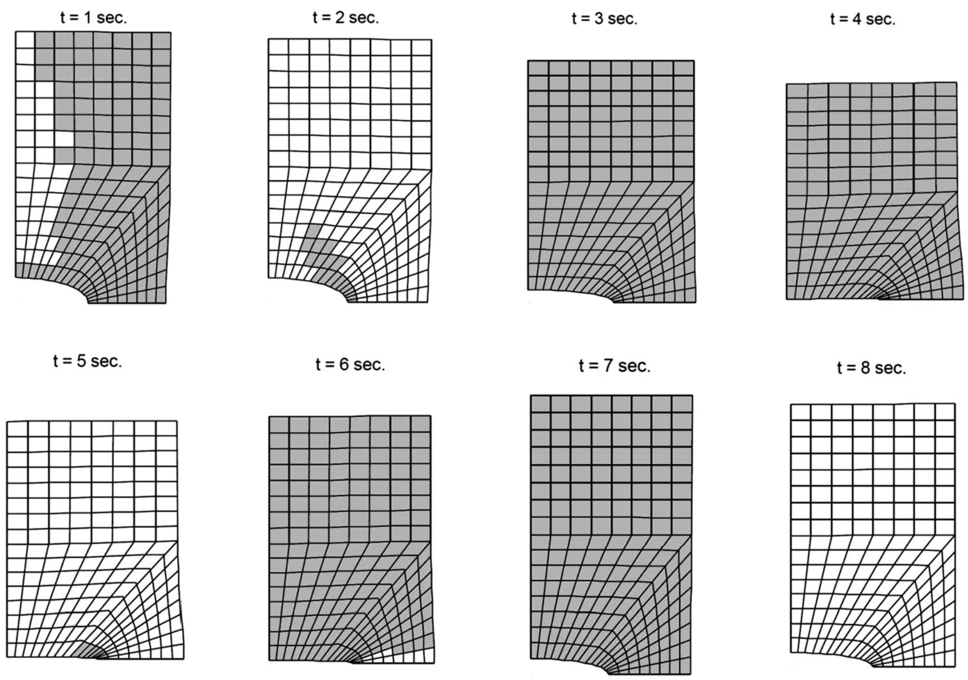

Fig. 24 The elements involvement in plastic computations alongside their deformations

Table 5 Residual norms of the tangent operators in a given finite-element analysis at increment 10th

Iteration	BE	FE	EXF	EXS
1	$1.1411 \times 10^{+3}$	$1.1411 \times 10^{+3}$	$1.1411 \times 10^{+3}$	$1.1411 \times 10^{+3}$
2	$1.2466 \times 10^{+2}$	$1.2471 \times 10^{+2}$	$1.2440 \times 10^{+2}$	$1.2441 \times 10^{+2}$
3	8.3437×10^{-1}	9.2663×10^{-1}	8.7046×10^{-1}	8.7138×10^{-1}
4	6.0179×10^{-3}	4.9443×10^{-3}	4.2676×10^{-3}	4.3732×10^{-3}
5	9.7430×10^{-5}	3.7380×10^{-5}	2.6812×10^{-5}	3.0949×10^{-5}
6	—	—	—	—

Table 6 Residual norms of the tangent operators in a given finite-element analysis at increment 60th

Iteration	BE	FE	EXF	EXS
1	$1.4764 \times 10^{+3}$	$1.4764 \times 10^{+3}$	$1.4764 \times 10^{+3}$	$1.4764 \times 10^{+3}$
2	$1.2888 \times 10^{+2}$	$1.1761 \times 10^{+2}$	$1.2744 \times 10^{+2}$	$1.2845 \times 10^{+2}$
3	9.4753×10^{-1}	$1.44761 \times 10^{+0}$	$1.5175 \times 10^{+0}$	$1.5270 \times 10^{+0}$
4	8.5521×10^{-3}	3.5782×10^{-2}	1.9349×10^{-2}	1.9299×10^{-2}
5	7.7426×10^{-5}	1.0564×10^{-3}	3.4564×10^{-4}	3.4306×10^{-4}
6	—	3.5646×10^{-5}	—	—

Table 7 The accuracy, computational time, and performance of the schemes in a boundary value problem

Integrating scheme	N_{inc}	E_T	$T_{CPU}(s)$	n_{it}	η	$\eta_n = \frac{\eta}{\eta_{BE}}$
BE	5	0.0882	178.05	5	0.064	1
	10	0.0461	328.92	5	0.066	1
FE	5	0.3282	259.47	12	0.012	0.18
	10	0.1342	386.37	9	0.019	0.28
EXF	5	0.0028	169.88	7	2.102	32.84
	10	0.0013	304.82	6	2.524	38.24
EXS	5	0.0008	215.22	7	5.808	90.75
	10	0.0002	393.61	6	12.703	192.47

independent strategy alongside the Newton–Raphson solution, an implicit nonlinear finite-element code is provided by the authors to compare the precision, computational effort and efficiency of the suggested integrations with the Euler's, likewise, better verifying the consistent tangent operators. The typical boundary value problem of a rectangular strip with a central elliptical opening is opted under the plane strain conditions. As it is shown in Fig. 21, the strip undergoes symmetric uniform loads applied perpendicularly on its all sides. Obviously, only one-quarter of the strip needs to be analyzed owing to its symmetry, see Fig. 21.

Assuming the thickness of unit for the strip, the quarter is discretized by 192 four-node isoparametric bilinear quadrilaterals as if displayed in Fig. 22. Furthermore, the biaxial nonproportional load history depicted in Fig. 23 is considered for the analyses. To better present the problem, the deformation of the strip and the elements endured plastic deformation are featured in Fig. 24 for the successive times of $t = 1 - 8\,\text{s}$. The elements having plastic strain are also depicted in Fig. 24 by gray color to see their involvements in plastic computations. Note that the displacements have been enlarged 50 times to be easily discernible. Moreover, the quadratic convergence rate of the tangent moduli are demonstrated deriving the Euclidian norm of the out-of-balance forces of Newton's iterations, which are presented in Tables 5 and 6 for two given increments of 10th and 60th.

Accuracy is defined as the inverse of the total error. To assess the accuracy of the algorithms, the total errors of nodes' displacements are computed through the following relationship:

$$E_T = \sum_{i=1}^{N} \frac{\left\| \mathbf{u}_j^{E} - \mathbf{u}_j^{N} \right\|}{\left\| \mathbf{u}_j^{E} \right\|} \text{ with } \mathbf{u}^{T} = \{u_1, u_2, \ldots, u_{node}\} \text{ and } u_i = \sqrt{u_{x,i}^2 + u_{y,i}^2} \qquad (141)$$

in which, N stands for the total number of load increments. The vector $\mathbf{u}_j^{E}$ specifies the reference global displacements of the nodes in jth increment computed by 100 subincrements. Additionally, $\mathbf{u}_j^{N}$ denotes the global displacement vector when the proposed and classical schemes are employed.

The total CPU times are also recorded to evaluate the formulations' speed during the finite-element analyses. Eventually, hiring

Downloaded From: http://materialstechnology.asmedigitalcollection.asme.org/ on 05/25/2013 Terms of Use: http://asme.org/terms

the same procedure as used in the stress-updating tests, the computational efficiency or performance is appraised employing Eq. (138) with the difference of using total error, E_{T}, instead of average error, E_{A}. Table 7 delivers the results for two numbers of subincrements; $N_{\mathrm{inc}} = 5$ and 10. To better interpret the results, the maximum number of iterations during each analysis is also added to the table represented by n_{it}.

Overall, the same results as observed in the stress and strain-updating tests are beheld here, too. Clearly, the tangent operators are working properly where the residual forces plunge down from 10^{+3} to 10^{-5} with the iterations as few as 5 or 6, see Tables 5 and 6. In case of the accuracy and computational efficiency assessments presented in Table 7, the first thing obvious is the considerable influence of the integration procedures on the outcomes of a small simple finite-element problem. This could surely intensify in almost all other pragmatic engineering problems for the plasticity computations that must be carried out in each Gauss point whose numbers soar as the structures become bigger and more complicated. Unquestionably, the most promising strategies in integrating the constitutive equations of the plasticity are the exponential-based methods. The EXF and EXS are far more accurate and efficient than the BE and FE. Among the exponentials, the EXS features great performance having an incredible precision alongside quadratic convergence rate.

7 Conclusions

A nonassociative plasticity model of Drucker–Prager's yield criterion along with nonlinear kinematic hardening is taken into consideration in which the plastic deformation is incompressible. This plasticity model was chosen since it fits the plastic behavior of a broad range of engineering metallic materials, specially DRA composites and many others like high-strength steel, aluminum, plain carbon, titanium, etc., as it was demonstrated by Lei and Lissenden [14].

Two consistent exponential-based formulations were proposed for integrating the constitutive equations of the plasticity model. These techniques, for short called EXF and EXS, have only been developed up to linear hardening and no hardening, respectively. In this investigation, they were evolved for the generalized nonlinear kinematic hardening. To verify the EXF and EXS, formulas of forward and backward Euler methods, FE and BE, were derived and briefly presented corresponding to the plasticity model. The vantage of EXS is to use better estimations of the stress and the yield-surface's features in each incremental step of the numerical procedure. A broad set of numerical tests were adopted to assess the integrating strategies in three major areas of accuracy, convergence rate, and computational efficiency or performance. After purely evaluating the schemes by the stress and strain histories at a given Gauss point, a typical boundary value problem was also solved implementing each technique in order to exhibit their performance in a real practice.

The greater accuracy and performance of the exponential-based tactics, especially the EXS, were obvious in the tests. It was also discerned that the EXS has second-order accuracy, which generates an increasing efficiency, whereas the EXF linearly approaches to the exact solution. Moreover, the direct correlation between the accuracy and efficiency of the integration schemes and the precision and computational effort of the nonlinear finite-element analyses were also obvious in the boundary value problem. As it was observed, the finite-element analyses performed using the exponential-based schemes were much more accurate and efficient than those carried out through the forward and backward Euler's techniques.

The consistent tangent moduli of the proposed and Eulers' methodologies were also developed to achieve the quadratic convergence rate when used in nonlinear finite-element analyses through a Newton algorithm. In order for the tangent operators to be examined, two diverse stress histories were chosen as well as the boundary value problem. For each stress history, the updated strains via the tangent operators of the EXF and EXS were derived and compared to those of FE and BE. Much more accurate strains by the EXF and EXS were concluded than FE and BE. Furthermore, having computed the relative Euclidean errors of the stress histories and the residual forces of the nonlinear finite-element analysis, the quadratic convergence rates through all developed tangent operators were proven, too.

In short, while the exponential-based integrations are explicit strategies with great speed and easy implementation, they have the advantages of the implicit tactics such as appreciable robustness and consistency with the yield surface and therefore, they are highly recommended for the finite-element codes.

Nomenclature

$\mathbf{a}$ = back stress tensor
$\mathbb{A}$ = control matrix
E = Young's modulus
E_{T} = total error
E_{A} = average error
$E^{\sigma}, E^{\varepsilon}$ = relative stress error, relative strain error
$\mathbf{e}, \mathbf{e}^{\mathrm{e}}, \mathbf{e}^{\mathrm{p}}$ = deviatoric strain tensor, elastic deviatoric strain tensor, plastic deviatoric strain tensor
F = yield-surface function
$G, \bar{G}$ = shear modulus, extended shear modulus
$\mathbb{G}$ = exponential/factor matrix
$H_{\mathrm{kin}}, H_{\mathrm{nl}}$ = kinematic hardening moduli
$\mathbf{i}$ = array representation of second-order identity tensor
$\mathbb{I}$ = fourth-order symmetric identity tensor: $\mathbb{I}_{ijkl} = 1/2(\delta_{ik}\delta_{jl} + \delta_{il}\delta_{jk})$
$\mathbb{I}_{\mathrm{dev}}$ = deviatoric projection tensor: $\mathbb{I}_{\mathrm{dev}} = \mathbb{I} - 1/3(\mathbf{i}\mathbf{i}^{\mathrm{T}})$
K = bulk modulus
$\mathbf{n}$ = identity tensor of deviatoric stress
p, p' = volumetric/hydrostatic stress, volumetric/hydrostatic shifted stress
Q = plastic potential function
R = radius of yield surface
$\mathbf{s}, \mathbf{s}'$ = deviatoric stress tensor, deviatoric shifted stress tensor
$\mathbf{s}''$ = deviatoric shifted stress tensor prior to correction
t = pseudotime
T_{CPU} = CPU time
$\mathbf{u}$ = global displacement vector
X^0 = integrating factor
$\mathbf{X}$ = augmented stress vector
α = scalar separating elastic and elastoplastic parts of a load increment
$\boldsymbol{\alpha}$ = deviatoric back stress tensor
β = material constant in Drucker–Prager yield criterion
$\varepsilon_{y,0}$ = first yielding strain
ε_{v} = volumetric/hydrostatic strain
$\boldsymbol{\varepsilon}, \boldsymbol{\varepsilon}^{\mathrm{e}}, \boldsymbol{\varepsilon}^{\mathrm{p}}$ = strain tensor, elastic strain tensor, plastic strain tensor
$\dot{\gamma}$ = plastic multiplier
λ = discrete plastic multiplier
η = performance of a numerical integration
$\boldsymbol{\sigma}, \boldsymbol{\sigma}'$ = stress tensor, shifted stress tensor
ν = Poisson ratio
τ_y = yield stress in pure shear
ξ = indicator of the specified point at the middle of an elastoplastic load increment

Appendix A: Forward Euler Integration

As it is customary for the forward Euler algorithm, a trial solution is considered as

$$\mathbf{s}_{n+1}^{\mathrm{TR}} = \mathbf{s}_n + 2G\Delta\mathbf{e}, \quad \boldsymbol{\alpha}_{n+1}^{\mathrm{TR}} = \boldsymbol{\alpha}_n, \quad \mathbf{s}_{n+1}^{\prime\mathrm{TR}} = \mathbf{s}_{n+1}^{\mathrm{TR}} - \boldsymbol{\alpha}_{n+1}^{\mathrm{TR}},$$
$$p_{n+1}^{\prime\mathrm{TR}} = p'_n + K\Delta\varepsilon_{\mathrm{v}}, \quad \tau_{\mathrm{y},n+1}^{\mathrm{TR}} = \tau_{\mathrm{y},n} \tag{A1}$$

The trial solution is admissible so long as the coming condition is met

Downloaded From: http://materialstechnology.asmedigitalcollection.asme.org/ on 05/25/2013 Terms of Use: http://asme.org/terms

$$\|\mathbf{s}'^{\mathrm{TR}}_{n+1}\| \le R^{\mathrm{TR}}_{n+1} = \sqrt{2}(\tau_{y,n+1} - \beta p'^{\mathrm{TR}}_{n+1}), \tag{A2}$$

otherwise, the strain increment involves a plastic portion to be specified. The next equalities give the information where α and $1-\alpha$ designate the elastic and plastic parts, respectively

$$\alpha = \frac{\sqrt{B^2 - 4AC} - B}{2A} \text{ with}$$
$$\begin{cases} A = 4G^2 \Delta\mathbf{e}^{\mathrm{T}} \Delta\mathbf{e} - 2(\beta K \Delta\varepsilon_{\mathrm{v}})^2 \\ B = 4G\Delta\mathbf{e}^{\mathrm{T}}\mathbf{s}'_n + 4\beta K(\tau_{\mathrm{y},n} - \beta p'_n)\Delta\varepsilon_{\mathrm{v}}, \quad \alpha \in [0,1) \\ C = \mathbf{s}'^{\mathrm{T}}_n \mathbf{s}'_n - 2(\tau_{\mathrm{y},n} - \beta p'_n)^2 \end{cases} \tag{A3}$$

Using the parameter α, the deviatoric and volumetric parts of the shifted stress are calculated at the turning point of the load step from elastic to plastic, as follows:

$$\mathbf{s}'_{n+\alpha} = \mathbf{s}'_n + 2G\alpha\Delta\mathbf{e} \tag{A4}$$

$$p'_{n+\alpha} = p'_n + K\alpha\Delta\varepsilon_{\mathrm{v}} \tag{A5}$$

The plastic multiplier is acquired via Eq. (50). Having computed λ and used Eqs. (13), (17), (18), (21), (22), and (27), the parameters are updated as follows:

$$\mathbf{s}'_{n+1} = \mathbf{s}'_{n+\alpha} + 2G(1-\alpha)\Delta\mathbf{e} - 2\bar{G}\lambda\mathbf{s}'_{n+\alpha} + \lambda\sum_{i=1}^{m} H_{\mathrm{nl},i}\boldsymbol{\alpha}_{n,i} \tag{A6}$$

$$p'_{n+1} = p'_{n+\alpha} + K(1-\alpha)\Delta\varepsilon_{\mathrm{v}} \tag{A7}$$

$$\tau_{\mathrm{y},n+1} = \tau_{\mathrm{y},n} = \tau_{\mathrm{y},0} \tag{A8}$$

$$\boldsymbol{\alpha}_{n+1} = \boldsymbol{\alpha}_n + \sum_{i=1}^{m}\left(H_{\mathrm{kin},i}\Delta\mathbf{e}^{\mathrm{p}} - H_{\mathrm{nl},i}\lambda\boldsymbol{\alpha}_{n,i}\right) \quad \text{with} \quad \Delta\mathbf{e}^{\mathrm{p}} = \lambda\mathbf{s}'_{n+\alpha} \tag{A9}$$

To enforce the consistency of the yield condition, the following corrector vector is required:

$$a_{\mathrm{f}} = \sqrt{(\mathbf{n}^{\mathrm{T}}_{n+1}\mathbf{s}'_{n+1})^2 - \|\mathbf{s}'_{n+1}\|^2 + 2(\tau_{\mathrm{y},n+1} - \beta p'_{n+1})^2} - \mathbf{n}^{\mathrm{T}}_{n+1}\mathbf{s}'_{n+1}, \quad \mathbf{n}_{n+1} = \frac{\mathbf{s}'_{n+1}}{\|\mathbf{s}'_{n+1}\|} \tag{A10}$$

$$\mathbf{s}'_{n+1} = \mathbf{s}'_{n+1} + a_{\mathrm{f}}\mathbf{n}_{n+1} \tag{A11}$$

Appendix B: Backward Euler Integration

The trial solution, Eq. (A1), and the associated condition, Eq. (A2), are utilized pursuing the scheme. If the tentative assumption is rejected, a plastic corrector is needed. The correction is executed by omitting the plastic part from the strain increment while calculating the stresses. Consequently, the variables are computed through the subsequent relationships

$$\mathbf{s}'_{n+1} = \mathbf{s}'^{\mathrm{TR}}_{n+1} - 2\bar{G}\lambda\mathbf{s}'_{n+1} + \lambda\sum_{i=1}^{m} H_{\mathrm{nl},i}\boldsymbol{\alpha}_{n+1,i} \rightarrow \mathbf{s}'_{n+1} = \frac{1}{(1+2\bar{G}\lambda)}\left(\mathbf{s}'^{\mathrm{TR}}_{n+1} + \lambda\sum_{i=1}^{m} H_{\mathrm{nl},i}\boldsymbol{\alpha}_{n+1,i}\right) \tag{B1}$$

$$\Delta\varepsilon^{\mathrm{p}}_{\mathrm{v}} = 0 \rightarrow p'_{n+1} = p'^{\mathrm{TR}}_{n+1} = p'_n + K\Delta\varepsilon_{\mathrm{v}} \tag{B2}$$

Equation (18) is hired to update the back stress vector, as follows:

$$\boldsymbol{\alpha}_{n+1,i} = \frac{\boldsymbol{\alpha}_{n,i}}{1 + H_{\mathrm{nl},i}\lambda} + \frac{H_{\mathrm{kin},i}\lambda}{1 + H_{\mathrm{nl},i}\lambda}\mathbf{s}'_{n+1} \tag{B3}$$

Replacing $\boldsymbol{\alpha}_{n+1,i}$ in Eq. (B1) with the former expression gives rise to the next relationship for $\mathbf{s}'_{n+1}$

$$\mathbf{s}'_{n+1} = \mathbf{s}'^{\mathrm{TR}}_{n+1} - 2\bar{G}\lambda\mathbf{s}'_{n+1} + \lambda\sum_{i=1}^{m}\frac{H_{\mathrm{nl},i}\boldsymbol{\alpha}_{n,i}}{1+\lambda H_{\mathrm{nl},i}} + \lambda^2\sum_{i=1}^{m}\frac{H_{\mathrm{nl},i}H_{\mathrm{kin},i}}{1+\lambda H_{\mathrm{nl},i}}\mathbf{s}'_{n+1} \tag{B4}$$

Using the yield function and substituting Eqs. (B2) and (B4) for $\mathbf{s}'_{n+1}$ and p'_{n+1} leads to the following equality from which λ is acquired:

$$\left(1 + 2\bar{G}\lambda - \lambda^2\sum_{i=1}^{m}\frac{H_{\mathrm{nl},i}H_{\mathrm{kin},i}}{1+\lambda H_{\mathrm{nl},i}}\right)^{-2}\left\|\mathbf{s}'^{\mathrm{TR}}_{n+1} + \lambda\sum_{i=1}^{m}\frac{H_{\mathrm{nl},i}\boldsymbol{\alpha}_{n,i}}{1+\lambda H_{\mathrm{nl},i}}\right\|^2 - R^2_{n+1} = 0, \quad R_{n+1} = \sqrt{2}(\tau_{\mathrm{y},0} - \beta p'_{n+1}) \tag{B5}$$

A root finding technique such as the Newton–Raphson method is hired to find the plastic multiplier.

Appendix C: Demonstration of Taking the Derivative of Stress With Respect to Strain, $\partial\boldsymbol{\sigma}_{n+1}/\partial\boldsymbol{\varepsilon}_{n+1}$

$$\boldsymbol{\sigma}_{n+1} = \mathbf{s}_{n+1} + p_{n+1}\mathbf{i} \quad \& \quad \mathbf{s}_{n+1} = \mathbf{s}'_{n+1} + \boldsymbol{\alpha}_{n+1} \tag{C1}$$

$$\frac{\partial\boldsymbol{\sigma}_{n+1}}{\partial\boldsymbol{\varepsilon}_{n+1}} = \frac{\partial\mathbf{s}'_{n+1}}{\partial\boldsymbol{\varepsilon}_{n+1}} + \frac{\partial\boldsymbol{\alpha}_{n+1}}{\partial\boldsymbol{\varepsilon}_{n+1}} + \frac{\partial(p_{n+1}\mathbf{i})}{\partial\boldsymbol{\varepsilon}_{n+1}} \tag{C2}$$

where the components of the last equation are calculated, as follows:

$$\begin{aligned} \frac{\partial\mathbf{s}'_{n+1}}{\partial\boldsymbol{\varepsilon}_{n+1}} &= \frac{\partial\mathbf{s}'_{n+1}}{\partial\mathbf{e}_{n+1}}\cdot\frac{\partial\mathbf{e}_{n+1}}{\partial\boldsymbol{\varepsilon}_{n+1}} = \frac{\partial\mathbf{s}'_{n+1}}{\partial\mathbf{e}_{n+1}}\cdot\mathbb{I}_{\mathrm{dev}} \\ \frac{\partial\boldsymbol{\alpha}_{n+1}}{\partial\boldsymbol{\varepsilon}_{n+1}} &= \frac{\partial\boldsymbol{\alpha}_{n+1}}{\partial\mathbf{e}_{n+1}}\cdot\frac{\partial\mathbf{e}_{n+1}}{\partial\boldsymbol{\varepsilon}_{n+1}} = \frac{\partial\boldsymbol{\alpha}_{n+1}}{\partial\mathbf{e}_{n+1}}\cdot\mathbb{I}_{\mathrm{dev}}, \quad \frac{\partial(p_{n+1}\mathbf{i})}{\partial\boldsymbol{\varepsilon}_{n+1}} = K(\mathbf{i}\mathbf{i}^{\mathrm{T}}) \end{aligned} \tag{C3}$$

Appendix D: Derivatives Mentioned in the Consistent Tangent Modulus of Forward Euler Method

The derivatives of $\mathbf{s}'_{n+\alpha}$, α, and λ are obtained in the following way:

$$\frac{\partial\mathbf{s}'_{n+\alpha}}{\partial\mathbf{e}_{n+1}} = 2G\left(\alpha + \frac{\partial\alpha}{\partial\mathbf{e}_{n+1}}\Delta\mathbf{e}^{\mathrm{T}}\right) \tag{D1}$$

$$\frac{\partial\alpha}{\partial\mathbf{e}_{n+1}} = 8A_1G^2\Delta\mathbf{e} + 4A_2G\mathbf{s}'_n \tag{D2}$$

$$A_1 = \left(\frac{1}{2}\right)\frac{2AC - B^2 + B\sqrt{B^2-4AC}}{A^2\sqrt{B^2-4AC}} \tag{D3}$$

$$A_2 = \left(\frac{1}{2}\right)\frac{B - \sqrt{B^2-4AC}}{A\sqrt{B^2-4AC}} \tag{D4}$$

$$\begin{aligned} A &= \|2G\Delta\mathbf{e}\|^2 - 2(\beta K\Delta\varepsilon_{\mathrm{v}})^2 \\ B &= 4G\Delta\mathbf{e}^{\mathrm{T}}\mathbf{s}'_n + 4\beta K(\tau_{\mathrm{y},0} - \beta p'_n)\Delta\varepsilon_{\mathrm{v}} \\ C &= \|\mathbf{s}'_n\|^2 - 2(\tau_{\mathrm{y},0} - \beta p'_n)^2 \end{aligned} \tag{D5}$$

$$\lambda = \frac{(1-\alpha)(2G\Delta\mathbf{e}^{\mathrm{T}}\mathbf{s}'_{n+\alpha} + 2\beta K(\tau_{\mathrm{y},0} - \beta p'_{n+\alpha})\Delta\varepsilon_{\mathrm{v}})}{4\bar{G}(\tau_{\mathrm{y},0} - \beta p'_{n+\alpha})^2 - \mathbf{s}'^{\mathrm{T}}_{n+\alpha}\sum_{i=1}^{m}H_{\mathrm{nl},i}\boldsymbol{\alpha}_{n,i}} = \frac{V}{W} \tag{D6}$$

$$\frac{\partial\lambda}{\partial\mathbf{e}_{n+1}} = \frac{\frac{\partial V}{\partial\mathbf{e}_{n+1}}W - \frac{\partial W}{\partial\mathbf{e}_{n+1}}V}{W^2} \tag{D7}$$

$$\begin{aligned} \frac{\partial V}{\partial\mathbf{e}_{n+1}} = &-2G\Delta\mathbf{e}^{\mathrm{T}}\mathbf{s}'_{n+\alpha}\frac{\partial\alpha}{\partial\mathbf{e}_{n+1}} + 2G(1-\alpha)\left(\mathbf{s}'_{n+\alpha} + \frac{\partial\mathbf{s}'_{n+\alpha}}{\partial\mathbf{e}_{n+1}}\Delta\mathbf{e}\right) \\ &- 2\beta\mathrm{K}\Delta\varepsilon_{\mathrm{v}}\left((\tau_{\mathrm{y},0} - \beta p'_{n+\alpha})\frac{\partial\alpha}{\partial\mathbf{e}_{n+1}} + \beta(1-\alpha)\frac{\partial p'_{n+\alpha}}{\partial\mathbf{e}_{n+1}}\right) \end{aligned} \tag{D8}$$

Downloaded From: http://materialstechnology.asmedigitalcollection.asme.org/ on 05/25/2013 Terms of Use: http://asme.org/terms

$$\frac{\partial W}{\partial \mathbf{e}_{n+1}}=-8\bar{G}\beta(\tau_{y,0}-\beta p'_{n+\alpha})\frac{\partial p'_{n+\alpha}}{\partial \mathbf{e}_{n+1}}-\frac{\partial \mathbf{s}'_{n+\alpha}}{\partial \mathbf{e}_{n+\alpha}}\sum_{i=1}^{m}H_{\mathrm{nl},i}\boldsymbol{\alpha}_{n,i} \tag{D9}$$

where $\partial \mathbf{s}'_{n+\alpha}/\partial \mathbf{e}_{n+1}$ is known by Eq. (D1) and $\partial p'_{n+\alpha}/\partial \mathbf{e}_{n+1}$ is derived below

$$\frac{\partial p'_{n+\alpha}}{\partial \mathbf{e}_{n+1}}=K\Delta\varepsilon_{\mathrm{v}}\frac{\partial \alpha}{\partial \mathbf{e}_{n+1}} \tag{D10}$$

Appendix E: Derivatives Mentioned in the Consistent Tangent Modulus of Fully Explicit Exponential Map Method

$\partial\Delta\hat{\boldsymbol{\mu}}/\partial \mathbf{e}_{n+1}$ is figured by hiring Eqs. (46) and (47), as follows:

$$\frac{\partial \Delta\hat{\boldsymbol{\mu}}}{\partial \mathbf{e}_{n+1}}=\frac{1}{\|\Delta\boldsymbol{\mu}\|}\frac{\partial \Delta\boldsymbol{\mu}}{\partial \mathbf{e}_{n+1}}-\frac{\Delta\boldsymbol{\mu}}{\|\Delta\boldsymbol{\mu}\|^3}\left(\frac{\partial \Delta\boldsymbol{\mu}}{\partial \mathbf{e}_{n+1}}\Delta\boldsymbol{\mu}\right)^{\mathrm{T}} \tag{E1}$$

$$\frac{\partial \Delta\boldsymbol{\mu}}{\partial \mathbf{e}_{n+1}}=(1-\alpha)\mathbb{I}-\Delta\mathbf{e}\left(\frac{\partial \alpha}{\partial \mathbf{e}_{n+1}}\right)^{\mathrm{T}}+\frac{1}{2G}\sum_{i=1}^{m}H_{\mathrm{nl},i}\boldsymbol{\alpha}_{n,i}\left(\frac{\partial \lambda}{\partial \mathbf{e}_{n+1}}\right)^{\mathrm{T}} \tag{E2}$$

$\partial a_{n+\alpha}/\partial \mathbf{e}_{n+1}$ and $\partial b_{n+\alpha}/\partial \mathbf{e}_{n+1}$ are also derived using Eqs. (48) and (49). The next results will be obtained

$$\frac{\partial a_{n+\alpha}}{\partial \mathbf{e}_{n+1}}=\frac{2G}{R_{n+\alpha}}\left(\frac{\partial \Delta\boldsymbol{\mu}}{\partial \mathbf{e}_{n+1}}\frac{\Delta\boldsymbol{\mu}}{\|\Delta\boldsymbol{\mu}\|}-\frac{\|\Delta\boldsymbol{\mu}\|}{R_{n+\alpha}}\frac{\partial R_{n+\alpha}}{\partial \mathbf{e}_{n+1}}\right)\sinh\left(\frac{2G}{R_{n+\alpha}}\|\Delta\boldsymbol{\mu}\|\right) \tag{E3}$$

$$\frac{\partial b_{n+\alpha}}{\partial \mathbf{e}_{n+1}}=\frac{2G}{R_{n+\alpha}}\left(\frac{\partial \Delta\boldsymbol{\mu}}{\partial \mathbf{e}_{n+1}}\frac{\Delta\boldsymbol{\mu}}{\|\Delta\boldsymbol{\mu}\|}-\frac{\|\Delta\boldsymbol{\mu}\|}{R_{n+\alpha}}\frac{\partial R_{n+\alpha}}{\partial \mathbf{e}_{n+1}}\right)\cosh\left(\frac{2G}{R_{n+\alpha}}\|\Delta\boldsymbol{\mu}\|\right) \tag{E4}$$

$$\frac{\partial R_{n+\alpha}}{\partial \mathbf{e}_{n+1}}=-\sqrt{2}\beta K\Delta\varepsilon_{\mathrm{v}}\frac{\partial \alpha}{\partial \mathbf{e}_{n+1}} \tag{E5}$$

It should be noted that $\partial\lambda/\partial \mathbf{e}_{n+1}$ and $\partial\alpha/\partial \mathbf{e}_{n+1}$ have already been presented in Appendix D.

Appendix F: Derivatives Mentioned in the Consistent Tangent Modulus of Semi-Implicit Exponential Map Method

$\partial \mathbf{X}^{\mathrm{S}}_{n+\alpha}/\partial \mathbf{e}_{n+1}$ and $\partial X^{\mathrm{R}}_{n+\alpha}/\partial \mathbf{e}_{n+1}$ are calculated by equalities (120) and (121). $\partial\Delta\hat{\boldsymbol{\mu}}^{\xi}_{n+\alpha}/\partial \mathbf{e}_{n+1}$ is obtained using relationships (68) and (69), as follows:

$$\frac{\partial \Delta\hat{\boldsymbol{\mu}}^{\xi}_{n+\alpha}}{\partial \mathbf{e}_{n+1}}=\frac{1}{\left\|\Delta\boldsymbol{\mu}^{\xi}_{n+\alpha}\right\|}\frac{\partial \Delta\boldsymbol{\mu}^{\xi}_{n+\alpha}}{\partial \mathbf{e}_{n+1}}-\frac{\Delta\boldsymbol{\mu}^{\xi}_{n+\alpha}}{\left\|\Delta\boldsymbol{\mu}^{\xi}_{n+\alpha}\right\|^3}\left(\frac{\partial \Delta\boldsymbol{\mu}^{\xi}_{n+\alpha}}{\partial \mathbf{e}_{n+1}}\Delta\boldsymbol{\mu}^{\xi}_{n+\alpha}\right)^{\mathrm{T}} \tag{F1}$$

$$\frac{\partial \Delta\boldsymbol{\mu}^{\xi}_{n+\alpha}}{\partial \mathbf{e}_{n+1}}=\xi(1-\alpha)\mathbb{I}-\xi\Delta\mathbf{e}\left(\frac{\partial \alpha}{\partial \mathbf{e}_{n+1}}\right)^{\mathrm{T}}+\frac{1}{2G}\sum_{i=1}^{m}H_{\mathrm{nl},i}\boldsymbol{\alpha}_{n,i}\left(\frac{\partial \lambda^{\xi}_{n+\alpha}}{\partial \mathbf{e}_{n+1}}\right)^{\mathrm{T}} \tag{F2}$$

where $\partial\alpha/\partial \mathbf{e}_{n+1}$ has already been calculated through Eqs. (D2)–(D5). $\partial\lambda^{\xi}_{n+\alpha}/\partial \mathbf{e}_{n+1}$ is also derived utilizing Eq. (70) which results in the relationships like (D6)–(D9) except for the below fact that there should be the factor ξ multiplied to these relationships

$$\frac{\partial \lambda^{\xi}_{n+\alpha}}{\partial \mathbf{e}_{n+1}}=\xi\frac{\partial \lambda_{n+\alpha}}{\partial \mathbf{e}_{n+1}} \tag{F3}$$

To derive $\partial a^{\xi}_{n+\alpha}/\partial \mathbf{e}_{n+1}$ and $\partial b^{\xi}_{n+\alpha}/\partial \mathbf{e}_{n+1}$, one can use Eq. (71) which contribute to the below equalities

$$\frac{\partial a^{\xi}_{n+\alpha}}{\partial \mathbf{e}_{n+1}}=\frac{2G}{R_{n+\alpha}}\left(\frac{\partial \Delta\boldsymbol{\mu}^{\xi}_{n+\alpha}}{\partial \mathbf{e}_{n+1}}\frac{\Delta\boldsymbol{\mu}^{\xi}_{n+\alpha}}{\left\|\Delta\boldsymbol{\mu}^{\xi}_{n+\alpha}\right\|}-\frac{\left\|\Delta\boldsymbol{\mu}^{\xi}_{n+\alpha}\right\|}{R_{n+\alpha}}\frac{\partial R_{n+\alpha}}{\partial \mathbf{e}_{n+1}}\right)\times\sinh\left(\frac{2G}{R_{n+\alpha}}\left\|\Delta\boldsymbol{\mu}^{\xi}_{n+\alpha}\right\|\right) \tag{F4}$$

$$\frac{\partial b^{\xi}_{n+\alpha}}{\partial \mathbf{e}_{n+1}}=\frac{2G}{R_{n+\alpha}}\left(\frac{\partial \Delta\boldsymbol{\mu}^{\xi}_{n+\alpha}}{\partial \mathbf{e}_{n+1}}\frac{\Delta\boldsymbol{\mu}^{\xi}_{n+\alpha}}{\left\|\Delta\boldsymbol{\mu}^{\xi}_{n+\alpha}\right\|}-\frac{\left\|\Delta\boldsymbol{\mu}^{\xi}_{n+\alpha}\right\|}{R_{n+\alpha}}\frac{\partial R_{n+\alpha}}{\partial \mathbf{e}_{n+1}}\right)\times\cosh\left(\frac{2G}{R_{n+\alpha}}\left\|\Delta\boldsymbol{\mu}^{\xi}_{n+\alpha}\right\|\right) \tag{F5}$$

To achieve $\partial\Delta\mathbf{e}^{\mathrm{p}}_{n+\xi(1-\alpha)}/\partial \mathbf{e}_{n+1}$, one can employ Eqs. (76)–(78). Thus, the following results are obtained:

$$\frac{\partial \Delta\mathbf{e}^{\mathrm{p}}_{n+\xi(1-\alpha)}}{\partial \mathbf{e}_{n+1}}=\frac{-\sum_{i=1}^{m}\frac{\partial \bar{H}_i}{\partial \mathbf{e}_{n+1}}}{\left(2G+\sum_{i=1}^{m}\bar{H}_i\right)^2}\left(\mathbf{s}_n+G\Delta\mathbf{e}-\sum_{i=1}^{m}\bar{\mathbf{a}}_{n,i}-\mathbf{s}'_{n+\xi(1-\alpha)}\right)+\frac{1}{2G+\sum_{i=1}^{m}\bar{H}_i}\left(G\mathbb{I}-\sum_{i=1}^{m}\frac{\partial \bar{\mathbf{a}}_{n,i}}{\partial \mathbf{e}_{n+1}}-\frac{\partial \mathbf{s}'_{n+\xi(1-\alpha)}}{\partial \mathbf{e}_{n+1}}\right) \tag{F6}$$

$$\frac{\partial \bar{H}_i}{\partial \mathbf{e}_{n+1}}=\frac{-\frac{H_{\mathrm{nl},i}H_{\mathrm{kin},i}}{2}\cdot\frac{\partial \bar{\lambda}}{\partial \mathbf{e}_{n+1}}}{(1+H_{\mathrm{nl},i}\bar{\lambda}/2)^2},\quad \frac{\partial \bar{\mathbf{a}}_{n,i}}{\partial \mathbf{e}_{n+1}}=\frac{-H_{\mathrm{nl},i}\frac{\partial \bar{\lambda}}{\partial \mathbf{e}_{n+1}}\boldsymbol{\alpha}_{n,i}}{(1+H_{\mathrm{nl},i}\bar{\lambda}/2)^2},$$
$$\frac{\partial \bar{\lambda}}{\partial \mathbf{e}_{n+1}}=\frac{1}{2\bar{G}R_{n+\xi(1-\alpha)}X^0_{n+\xi(1-\alpha)}}\cdot\frac{\partial X^{\mathrm{R}}_{n+\xi(1-\alpha)}}{\partial \mathbf{e}_{n+1}} \tag{F7}$$

Using Eqs. (82) and (83), one can have the coming formulas

$$\frac{\partial \Delta\hat{\boldsymbol{\mu}}_{n+\xi(1-\alpha)}}{\partial \mathbf{e}_{n+1}}=\frac{1}{\left\|\Delta\boldsymbol{\mu}_{n+\xi(1-\alpha)}\right\|}\frac{\partial \Delta\boldsymbol{\mu}_{n+\xi(1-\alpha)}}{\partial \mathbf{e}_{n+1}}-\frac{\Delta\boldsymbol{\mu}_{n+\xi(1-\alpha)}}{\left\|\Delta\boldsymbol{\mu}_{n+\xi(1-\alpha)}\right\|^3}\left(\frac{\partial \Delta\boldsymbol{\mu}_{n+\xi(1-\alpha)}}{\partial \mathbf{e}_{n+1}}\Delta\boldsymbol{\mu}_{n+\xi(1-\alpha)}\right)^{\mathrm{T}} \tag{F8}$$

$$\frac{\partial \Delta\boldsymbol{\mu}_{n+\xi(1-\alpha)}}{\partial \mathbf{e}_{n+1}}=(1-\alpha)\mathbb{I}-\Delta\mathbf{e}\left(\frac{\partial \alpha}{\partial \mathbf{e}_{n+1}}\right)^{\mathrm{T}}+\frac{1}{2G}\sum_{i=1}^{m}H_{\mathrm{nl},i}\boldsymbol{\alpha}_{n+\xi(1-\alpha),i}\left(\frac{\partial \lambda_{n+\xi(1-\alpha)}}{\partial \mathbf{e}_{n+1}}\right)^{\mathrm{T}} \tag{F9}$$

where $\partial\lambda_{n+\xi(1-\alpha)}/\partial \mathbf{e}_{n+1}$ is obtained through Eqs. (D6)–(D9) substituting the subscript $n+\xi(1-\alpha)$ for $n+\alpha$. The derivatives $\partial \mathbf{X}^{\mathrm{S}}_{n+1}/\partial \mathbf{e}_{n+1}$ and $\partial X^{\mathrm{R}}_{n+1}/\partial \mathbf{e}_{n+1}$ are computed through the following relationships acquired from Eqs. (79) to (81):

$$\frac{\partial \mathbf{X}^{\mathrm{S}}_{n+1}}{\partial \mathbf{e}_{n+1}}=\frac{\partial \mathbf{X}^{\mathrm{S}}_{n+\alpha}}{\partial \mathbf{e}_{n+1}}+(\Delta\hat{\boldsymbol{\mu}}^{\mathrm{T}}_{n+\xi(1-\alpha)}\mathbf{X}^{\mathrm{S}}_{n+\alpha})\Delta\hat{\boldsymbol{\mu}}_{n+\xi(1-\alpha)}\left(\frac{\partial a_{n+\xi(1-\alpha)}}{\partial \mathbf{e}_{n+1}}\right)^{\mathrm{T}}+\Delta\hat{\boldsymbol{\mu}}_{n+\xi(1-\alpha)}\left((a_{n+\xi(1-\alpha)}-1)\mathbf{Q}'_1+\mathbf{Q}'_2\right)^{\mathrm{T}}+\left((a_{n+\xi(1-\alpha)}-1)(\Delta\hat{\boldsymbol{\mu}}^{\mathrm{T}}_{n+\xi(1-\alpha)}\mathbf{X}^{\mathrm{S}}_{n+\alpha})+b_{n+\xi(1-\alpha)}X^{\mathrm{R}}_{n+\alpha}\right)\times\frac{\partial \Delta\hat{\boldsymbol{\mu}}_{n+\xi(1-\alpha)}}{\partial \mathbf{e}_{n+1}} \tag{F10}$$

Downloaded From: http://materialstechnology.asmedigitalcollection.asme.org/ on 05/25/2013 Terms of Use: http://asme.org/terms

$$\mathbf{Q}_1' = \left(\frac{\partial \Delta\hat{\boldsymbol{\mu}}_{n+\xi(1-\alpha)}}{\partial \mathbf{e}_{n+1}}\mathbf{X}^{\mathrm{S}}_{n+\alpha} + \frac{\partial \mathbf{X}^{\mathrm{S}}_{n+\alpha}}{\partial \mathbf{e}_{n+1}}\Delta\hat{\boldsymbol{\mu}}_{n+\xi(1-\alpha)}\right) \tag{F11}$$

$$\mathbf{Q}_2' = \left(\frac{\partial b_{n+\xi(1-\alpha)}}{\partial \mathbf{e}_{n+1}}X^{\mathrm{R}}_{n+\alpha} + b_{n+\xi(1-\alpha)}\frac{\partial X^{\mathrm{R}}_{n+\alpha}}{\partial \mathbf{e}_{n+1}}\right) \tag{F12}$$

$$\frac{\partial X^{\mathrm{R}}_{n+1}}{\partial \mathbf{e}_{n+1}} = \frac{\partial a_{n+\xi(1-\alpha)}}{\partial \mathbf{e}_{n+1}}X^{\mathrm{R}}_{n+\alpha} + a_{n+\xi(1-\alpha)}\frac{\partial X^{\mathrm{R}}_{n+\alpha}}{\partial \mathbf{e}_{n+1}} + b_{n+\xi(1-\alpha)}\mathbf{Q}_1' + \frac{\partial b_{n+\xi(1-\alpha)}}{\partial \mathbf{e}_{n+1}}(\Delta\hat{\boldsymbol{\mu}}^{\mathrm{T}}_{n+\xi(1-\alpha)}\mathbf{X}^{\mathrm{S}}_{n+\alpha}) \tag{F13}$$

In these relationships, $\partial \mathbf{X}^{\mathrm{S}}_{n+\alpha}/\partial \mathbf{e}_{n+1}$ and $\partial X^{\mathrm{R}}_{n+\alpha}/\partial \mathbf{e}_{n+1}$ have been calculated through Eqs. (120) and (121). $\partial\hat{\boldsymbol{\mu}}_{n+\xi(1-\alpha)}/\partial \mathbf{e}_{n+1}$, $\partial a_{n+\xi(1-\alpha)}/\partial \mathbf{e}_{n+1}$, and $\partial b_{n+\xi(1-\alpha)}/\partial \mathbf{e}_{n+1}$ are achieved through Eqs. (D6)–(E5) replacing subscript $n+\alpha$ with $n+\xi(1-\alpha)$ in which $\partial \mathbf{s}'_{n+\xi(1-\alpha)}/\partial \mathbf{e}_{n+1}$ is calculated by Eq. (127) and $\partial p'_{n+\xi(1-\alpha)}/\partial \mathbf{e}_{n+1}$ is obtained as follows:

$$p'_{n+\xi(1-\alpha)} = p'_n + (\alpha + \xi(1-\alpha))K\Delta\varepsilon_{\mathrm{v}} \tag{F14}$$

$$\frac{\partial p'_{n+\xi(1-\alpha)}}{\partial \mathbf{e}_{n+1}} = (1-\xi)K\Delta\varepsilon_{\mathrm{v}}\frac{\partial \alpha}{\partial \mathbf{e}_{n+1}} \tag{F15}$$

$\partial R_{n+\xi(1-\alpha)}/\partial \mathbf{e}_{n+1}$ is gained using relationships (72) and (F14), which has the below shape

$$\frac{\partial R_{n+\xi(1-\alpha)}}{\partial \mathbf{e}_{n+1}} = \sqrt{2}(\xi-1)\beta \mathrm{K}\Delta\varepsilon_{\mathrm{v}}\frac{\partial \alpha}{\partial \mathbf{e}_{n+1}} \tag{F16}$$

References

[1] Bridgman, P. W., 1947, "The Effect of Hydrostatic Pressure on the Fracture of Brittle Substances," J. Appl. Phys., **18**, pp. 246–258.
[2] Bridgman, P. W., 1952, *Studies in Large Plastic Flow and Fracture With Special Emphasis on the Effect of Hydrostatic Pressure*, McGraw-Hill, New York.
[3] Spitzig, W. A., Sober, R. J., and Richmond, O., 1975, "Pressure Dependence of Yielding and Associated Volume Expansion in Tempered Martensite," Acta Metall., **23**, pp. 885–893.
[4] Spitzig, W. A., Sober, R. J., and Richmond, O., 1976, "The Effect of Hydrostatic Pressure on the Deformation Behavior of Maraging and HY-80 and Its Implication for Plasticity," Metall. Trans. A, **A7**, pp. 457–463.
[5] Spitzig, W. A., and Richmond, O., 1984, "The Effect of Pressure on the Flow Stress of Metals," Acta Metall., **32**, pp. 457–463.
[6] Wilson, C. D., 2002, "A Critical Reexamination of Classical Metal Plasticity," ASME J. Appl. Mech., **69**, pp. 63–68.
[7] Drucker, D. C., and Prager, W., 1952, "Soil Mechanics and Plastic Analysis or Limit Design," Q. Appl. Math., **10**, pp. 157–165.
[8] Singh, A. P., Padmanabhan, K. A., Pandy, G. N., Murty, G. M. D., and Jha, S., 2000, "Strength Differential Effect in Four Commercial Steels," J. Mater. Sci., **35**, pp. 1379–1388.
[9] Altenbach, H., Stoychev, G. B., and Tushtev, K. N., 2001, "On Elastoplastic Deformation of Grey Cast Iron," Int. J. Plast., **17**, pp. 719–736.
[10] Chait, R., 1973, "The Strength Differential of Steel and Ti Alloys as Influenced by Test Temperature and Microstructure," Scr. Metall., **7**, pp. 351–363.
[11] Gil, C. M., Lissenden, C. J., and Lerch, B. A., 1999, "Yield of Inconel 718 by Axial-Torsional Loading at Temperatures Up to 649 °C," J. Test. Eval., **27**, pp. 327–336.
[12] Iyer, S. K., and Lissenden, C. J., 2000, "Initial Anisotropy of Inconel 718: Experiments and Mathematical Representation." J. Eng. Mater. Technol., **122**, pp. 321–326.
[13] Lewandowski, J. J., Wesseling, P., Prabhu, N. S., Larose, J., and Lerch, B. A., 2003, "Strength Differential Measurements in IN-718: Effects of Superimposed Pressure," Metall. Mater. Trans. A, **34A**, pp. 1736–1739.
[14] Lei, X., and Lissenden, C. J., 2007, "Pressure Sensitive Nonassociative Plasticity Model for DRA Composites," ASME J. Eng. Mater. Technol., **129**, pp. 255–264.
[15] Prager, W., 1956, "A New Method of Analyzing Stresses and Strains in Work Hardening Plastic Solids." ASME J. Appl. Mech., **23**, pp. 493–496.
[16] Chakrabarty, J., 2000, *Theory of Plasticity*, 3rd ed. Elsevier Butterworth-Heinemann, Oxford, UK.
[17] Bari, S., and Hassan, T., 2000, "Anatomy of Coupled Constitutive Models for Ratcheting Simulation," Int. J. Plast., **16**, pp. 381–409.
[18] Armstrong, P. J., and Frederick, C. O., 1966, "A Mathematical Representation of the Multiaxial Bauschinger Effect," CEGB Report No. RD/B/N 731.
[19] Chaboche, J. L., 1986, "Time-Independent Constitutive Theories for Cyclic Plasticity," Int. J. Plast., **2**, pp. 149–188.
[20] Chaboche, J. L., 1991, "On Some Modifications of Kinematic Hardening to Improve the Description of Ratcheting Effects," Int. J. Plast., **7**, pp. 661–678.
[21] Ohno, N., and Wang, J. D., 1993, "Kinematic Hardening Rules With Critical State of Dynamic Recovery—Part I: Formulations and Basic Features for Ratcheting Behavior," Int. J. Plast., **9**, pp. 375–390.
[22] Abdel-Karim, M., and Ohno, N., 2000, "Kinematic Hardening Model Suitable for Ratcheting With Steady-State," Int. J. Plast., **16**, pp. 225–240.
[23] Kang, G., 2004, "A Visco-Plastic Constitutive Model for Ratcheting of Cyclically Stable Materials and Its Finite Element Implementation," Mech. Mater., **36**, pp. 299–312.
[24] Chaboche, J. L., 2008, "A Review of Some Plasticity and Viscoplasticity Constitutive Theories," Int. J. Plast., **24**, pp. 1642–1693.
[25] Abdel-Karim, M., 2009, "Modified Kinematic Hardening Rules for Simulations of Ratcheting," Int. J. Plast., **25**, pp. 1560–1587.
[26] Rezaiee-Pajand, M., and Sinaie, S., 2009, "On the Calibration of the Chaboche Hardening Model and a Modified Hardening Rule for Uniaxial Ratcheting Prediction," Int. J. Solids Struct., **46**, pp. 3009–3017.
[27] Mroz, Z., 1967, "On the Description of Anisotropic Work Hardening," J. Mech. Phys. Solids, **15**, pp. 163–175.
[28] Dafalias, Y. F., and Popov, E. P., 1976, "Plastic Internal Variables Formalism of Cyclic Plasticity," ASME J. Appl. Mech., **43**, pp. 645–650.
[29] Tseng, N. T., and Lee, G. C., 1983, "Simple Plasticity Model of the Two-Surface Type," ASCE J. Eng. Mech., **109**, pp. 795–810.
[30] Krieg, R. D., and Krieg, D. B., 1977, "Accuracies of Numerical Solution Methods for the Elastic-Perfectly Plastic Model," ASME J. Pressure Vessel Technol., **99**, pp. 510–515.
[31] Yoder, P. J., and Whirley, R. G., 1984, "On the Numerical Implementation of Elastoplastic Models," ASME J. Appl. Mech., **51**, pp. 283–288.
[32] Loret, B., and Prevost, J. H., 1986, "Accurate Numerical Solutions for Drucker-Prager Elastic-Plastic Models," Comput. Methods Appl. Mech. Eng., **54**, pp. 259–277.
[33] Ristinmaa, M., and Tryding, J., 1993, "Exact Integration of Constitutive Equations in Elastoplasticity," Int. J. Numer. Methods Eng., **36**, pp. 2525–2544.
[34] Wei, Z., Perić, D., and Owen, D. R. J., 1996, "Consistent Linearization for the Exact Stress Update of Prandtl–Reuss Non-Hardening Elastoplastic Models," Int. J. Numer. Methods Eng., **39**, pp. 1219–1235.
[35] Szabó, L., 2009, "A Semi-Analytical Integration Method for J2 Flow Theory of Plasticity With Linear Isotropic Hardening," Comput. Methods Appl. Mech. Eng., **198**, pp. 2151–2166.
[36] Rezaiee-Pajand, M., Sharifian, M., and Sharifian, M., 2011, "Accurate and Approximate Integrations of Drucker-Parger Plasticity With Linear Isotropic and Kinematic Hardening," Eur. J. Mech. A/Solids, **30**, pp. 345–361.
[37] Rezaiee-Pajand, M., and Sharifian, M., 2012, "A Novel Formulation for Integrating Nonlinear Kinematic Hardening Drucker-Prager's Yield Condition," Eur. J. Mech. A/Solids, **31**, pp. 163–178.
[38] Wilkins, M. L., 1964, "Calculation of Elastic-Plastic Flow," *Methods in Computational Physics*, Vol. 3, Academic Press, New York.
[39] Rice, J. R., and Tracey, D. M., 1973, "Computational Fracture Mechanics," *Numerical and Computer Methods in Structural Mechanics*, S. J. Fenves, ed., Academic Press, New York, pp. 585–623.
[40] Ortiz, M., and Popov, E. P., 1985, "Accuracy and Stability of Integration Algorithms for Elastoplastic Constitutive Relations," Int. J. Numer. Methods Eng., **21**, pp. 1561–1576.
[41] Kobayashi, M., and Ohno, N., 2002, "Implementation of Cyclic Plasticity Models Based on a General Form of Kinematic Hardening," Int. J. Numer. Methods Eng., **53**, pp. 2217–2238.
[42] Kobayashi, M., Mukai, M., Takahashi, H., Ohno, N., Kawakami, T., and Ishikawa, T., 2003, "Implicit Integration and Consistent Tangent Modulus of a Time-Dependent Non-Unified Constitutive Model," Int. J. Numer. Methods Eng., **58**, pp. 1523–1543.
[43] Kang, G., 2006, "Finite Element Implementation of Viscoplastic Constitutive Model With Strain-Range Dependent Cyclic Hardening," Commun. Numer. Methods Eng., **22**(2), pp. 137–153.
[44] Kan, Q. H., Kang, G. Z., and Zhang, J., 2007, "A Unified Visco-Plastic Constitutive Model for Uniaxial Time-Dependent Ratchetting and Its Finite Element Implementation," Theor. Appl. Fract. Mech., **47**, pp. 133–144.
[45] Coombs, W. M., Crouch, R. S., and Augarde, C. E., 2010, "Reuleaux Plasticity: Analytical Backward Euler Stress Integration and Consistent Tangent," Comput. Methods Appl. Mech. Eng., **199**, pp. 1733–1743.
[46] Hong, H. K., and Liu, C. S., 1999, "Internal Symmetry in Bilinear Elastoplasticity," Int. J. Non-Linear Mech., **34**, pp. 279–288.
[47] Hong, H. K., and Liu, C. S., 2000, "Internal Symmetry in the Constitutive Model of Perfect Elastoplasticity," Int. J. Non-Linear Mech., **35**, pp. 447–466.
[48] Hong, H. K., and Liu, C. S., 2000, "Lorentz Group on Minkowski Spacetime for Construction of the Two Basic Principles of Plasticity." Int. J. Non-Linear Mech., **36**, pp. 679–686.
[49] Liu, C. S., 2003, "Symmetry Groups and the Pseudo-Riemann Spacetimes for Mixed-Hardening Elastoplasticity," Int. J. Solids Struct., **40**, pp. 251–269.
[50] Liu, C. S., 2004, "A Consistent Numerical Scheme for the Von-Mises Mixed-Hardening Constitutive Equations." Int. J. Plast., **20**, pp. 663–704.
[51] Liu, C. S., 2004, "Internal Symmetry Groups for the Drucker-Prager Material Model of Plasticity and Numerical Integrating Methods." Int. J. Solids Struct., **41**, pp. 3771–3791.
[52] Auricchio, F., and Beirão da Veiga, L., 2003, "On a New Integration Scheme for Von-Mises Plasticity With Linear Hardening," Int. J. Numer. Methods Eng., **56**, pp. 1375–1396.
[53] Artioli, E., Auricchio, F., and Beirão da Veiga, L., 2005, "Integration Schemes for Von-Mises Plasticity Models Based on Exponential Maps: Numerical

Downloaded From: http://materialstechnology.asmedigitalcollection.asme.org/ on 05/25/2013 Terms of Use: http://asme.org/terms

Investigations and Theoretical Considerations," Int. J. Numer. Methods Eng., **64**, pp. 1133–1165.
[54] Artioli, E., Auricchio, F., and Beirão da Veiga, L., 2006, "A Novel 'Optimal' Exponential-Based Integration Algorithm for Von-Mises Plasticity With Linear Hardening: Theoretical Analysis on Yield Consistency, Accuracy, Convergence and Numerical Investigations," Int. J. Numer. Methods Eng., **4**, pp. 449–498.
[55] Artioli, E., Auricchio, F., and Beirão da Veiga, L., 2007, "Second-Order Accurate Integration Algorithms for Von-Mises Plasticity With a Nonlinear Kinematic Hardening Mechanism," Comput. Methods Appl. Mech. Eng., **196**, pp. 1827–1846.
[56] Rezaiee-Pajand, M., and Nasirai, C., 2007, "Accurate Integration Scheme for Von-Mises Plasticity With Mixed-Hardening Based on Exponential Maps," Eng. Comput., **24**(6), pp. 608–635.
[57] Rezaiee-Pajand, M., and Nasirai, C., 2008, "On the Integration Schemes for Drucker-Prager's Elastoplastic Models Based on Exponential Maps." Int. J. Numer. Methods Eng., **74**, pp. 799–826.
[58] Rezaiee-Pajand, M., Nasirai, C., and Sharifian, M., 2010, "Application of Exponential-Based Methods in Integrating the Constitutive Equations With Multicomponent Kinematic Hardening," ASCE J. Eng. Mech., **136**(12), pp. 1502–1518.
[59] Rezaiee-Pajand, M., Nasirai, C., and Sharifian, M., 2011, "Integration of Nonlinear Mixed Hardening Models," Multidiscip. Model. Mater. Struct. **7**(3), pp. 266–305.
[60] de Souza Neto, E. A., Perić, D., and Owen, D. R. J., 2008, *Computational Methods for Plasticity: Theory and Applications*, John Wiley and Sons, Ltd, New York.

Downloaded From: http://materialstechnology.asmedigitalcollection.asme.org/ on 05/25/2013 Terms of Use: http://asme.org/terms